OUKA
Osaka University Knowledge Archive

Title	Quantitative analysis of cell-free synthesized membrane proteins at the droplet interface bilayer in a newly designed chamber
Author(s)	Elfaramawy, Maie
Citation	大阪大学, 2023, 博士論文
Version Type	VoR
URL	https://doi.org/10.18910/92908
rights	
Note	

Osaka University Knowledge Archive : OUKA

https://ir.library.osaka-u.ac.jp/

Osaka University

Doctoral Dissertation

Quantitative analysis of cell-free synthesized membrane proteins at the droplet interface bilayer in a newly designed chamber

Maie Ahmed Elfaramawy

May 2023

Biotechnology Global Human Resource Development Program,

Division of Advanced Science and Biotechnology,

Graduate School of Engineering,

Osaka University

Abstract

Membrane proteins are responsible for cellular sensing, signalling and transport which gave them high potential to be used for various biotechnology application, while they have hardly been used due to their difficulty of handling by conventional techniques. Overexpression of membrane proteins inside living cells often results in cell toxicity and aggregation. Conventional techniques of isolation and purification leads to loss of protein function and time consuming. An *in vitro* transcription-translation (IVTT) system has been used to rapidly synthesize the membrane protein (MP) of interest independent of living cells. MPs require hydrophobic environments to fold and exhibit their function, which can easily be provided by adding liposomes or detergents to an IVTT system. Among many strategies for providing hydrophobic environments to an IVTT system, Droplet Interface Bilayer (DIB) approach is one of the simplest ways of forming stable bilayers which has a potential to provide an environment for various proteins to be incorporated. DIB can be prepared by contacting two water-in-oil (w/o) droplet, where phospholipids are dissolved in the oil phase. Lipid bilayer appears between the two droplets. DIBs have several advantages for the study of MPs; smaller amounts of protein are required and does not require skilled operators. However, previous studies failed in making stable DIBs consist of an IVTT system. In addition, to the best of our knowledge, there have been no reports quantifying the number of synthesized MPs supplied to the DIB by an IVTT system, presumably due to DIB instability. In this study, I firstly investigated the experimental condition where a green fluorescent protein can be expressed inside DIB by using an IVTT system without disrupting the DIB. Secondly, I synthesized and quantified the amount of MPs localized at the DIB using fluorescence data derived from the function of MPs.

I focused on stabilizing the DIB made by a reconstituted IVTT system, namely the PURE system. For this purpose, I selected the suitable oil phase for preparing lipid dissolved oil solution that increase the formation and stability of DIB at 37 °C for at least 2 h, which is required for protein synthesis. I obtained the highest DIB formation efficiency and stability with a 20 mg/mL (DOPC) in mixture of 10: 1 (v/v) hexadecane to decane. I also found that the chamber design affects the droplet shape and DIB contact length. From three different chamber designs tested, round bottom V2 (RB2) stabilized the location of the droplet most and showed the highest stability during the incubation. Form these results, I concluded that the setup for stable DIB made of a w/o droplets consist of a reconstituted IVTT system is 20 mg/mL (DOPC) in a mixture of 10: 1 (v/v) hexadecane to decane inside RB2 chamber.

As a first example, I used α-hemolysin (AH) a pore-forming protein from *Staphylococcus aureus*, that is expressed as a soluble monomer and assembles into heptamer on the lipid membrane. AH was synthesized inside one of the w/o droplets using a reconstituted IVTT

system, and a small molecule (FDGlcU) was added to the IVTT solution to investigate the pore formation. The diffusion of FDGlcU through AH nanopore was confirmed, as FDGlcU first diffuse to the other droplet, and hydrolysed by β-glucuronidase to emit fluorescent signal. I quantified the amount of AH inserted into bilayer based on the fluorescent data. I obtained the number of pores N_{pore} = 4.8 x 10^4 heptamers per DIB, and the fraction of AH inserted into the bilayer was determined to be 2.4 x 10^{-6} % of the total amount of AH synthesized. As *in vitro* system is highly controllable and adjustable, it is possible to investigate various parameter affecting the AH insertion and consequence the fluorescence flux. As a demonstration, I investigated the effect of lipid composition and other parameters on AH pore formation. As AH is a soluble protein, the next step is to test the function and DIB localization of typical membrane proteins that are expressed in an insoluble fraction in the absence of lipids or detergents.

I synthesized, EmrE, a multidrug transporter from *Escherichia coli*, inside RB2 chamber using a reconstituted IVTT system, and quantified the amount of EmrE at the DIB based on the fluorescence signal. I found the fraction of EmrE inserted into bilayer was found to be 1.0 x 10^{-4} % of the total amount of EmrE dimers synthesized, which is 30-fold higher than that of AH. Note that the fraction of AH inserted into bilayer to that obtained using FDGlcU and EtBr flux were very similar, indicating the validity of our measurement. Finally, to demonstrate that observed EmrE function is not an artifact, I tested the EtBr flux inhibition using tetraphenylphosphonium (TPP^+), a very well-known substrate of EmrE, and calcein, an unrelated compound. I observed the inhibition of EtBr signal only with TPP^+, indicating that synthesized EmrE exhibit proper substrate specificity.

In summary, I was able to synthesize MPs using a reconstituted IVTT system and quantified the amount of MPs at the DIB inside the developed chamber that has been proved to aid in stabilizing the DIBs for at least 19 h. To show the potentiality of this method, I quantified two different type of MPs; the pore-forming protein (AH) and multidrug transporter EmrE. This study provides a platform for further improvement and understanding of how membrane proteins are integrated and function into the lipid bilayer using a bottom-up approach.

Contents

Abbreviations

AH	α-Hemolysin
Alexa 647	Alexa fluor 647
BSA-A488	Bovine serum albumin conjugated to AlexaFluor488
CHO	Cholesterol
DIB	Droplet interface bilayer
DOPC	1,2-Dioleoyl-*sn*-glycero-3-phosphocholine
EtBr	Ethidium bromide
FB	Flat-bottom
FDGlcU	Fluorescein di-β-D-glucuronide
GFP	Green fluorescent protein
GUS	β-Glucuronidase
IVTT	*In vitro* protein transcription-translation system
MPs	Membrane proteins
OA647	Ovalbumin conjugated to Alexa-Fluor647
PC	Phosphatidylcholine
PCR	Polymerase chain reaction
PDB	Protein data bank
RB1 chamber	Round-bottom V1 chamber
RB2 chamber	Round-bottom V2 chamber
RNasin	Ribonuclease inhibitor
SDS	Sodium dodecyl sulfate
SDS-PAGE	Sodium dodecyl sulfate - Polyacrylamide gel electrophoresis
SM	Sphingomyelin
SMR proteins	Small multidrug resistance proteins
TAlexa 647	Transferrin from Human Serum, Alexa Fluor 647 Conjugate
TPP^+	Tetraphenylphosphonium
tRNA	Transfer RNA
w/o droplets	Water-in-oil droplets

Chapter 1 General introduction

1-1 Importance and difficulties of studying membrane proteins

Membrane proteins (MPs) are importance for the survival of organisms and account for 20–30% of the cellular proteins [1]. MPs are outlined as proteins that are in contact to the lipid bilayer, which could entirely or partly span the membrane, or localized at the surface of the membrane [2]. MPs are typically classified into several groups including ion channels, membrane receptors and transporters. Ion channels are molecules that allow the ions to penetrate across the membrane. Receptors are molecules that binds to target molecules, which triggers intracellular signalling pathways. Transporters are molecules that transport small molecules and ions across the membrane, supplying essential nutrients and disposing cellular waste [2].

Despite their high potential for the use in various applications including biosensors, there are limited number of application of MPs in the field of biotechnology due to their difficulty in isolation and purification of functional MPs [3]. Conventional cell-based strategies concentrate on over-expression in particular cells often resulting in little membrane insertion, aggregation, and/or may exhibit toxicity because of the alterations of the host cell's metabolism [4]. Additionally, when expressed as a recombinant, unnatural modification such as glycosylation, methylation and acetylation may occur.

Because MPs are important in understanding various behaviour of the cells, researcher have tried to study the structure-function relationship of various membrane proteins. After

decades of studies, it has become clear that purifying the MPs in their functional form is far more difficult compared to that of the soluble proteins [3], which is also reflected in the number of identified three dimensional structure of proteins: while 160,000 structures are present in the PDB, only about 2-3% are membrane proteins. These results strongly suggest the difficulties in working and utilizing MPs.

As far as I am concerned, nanopore sequencing developed by Oxford Nanopore (MinION), which is a novel DNA sequencing technology, is the only commercially available product which utilized one of the MPs, CsgG [5] from *E.coli* as an element.

1-2 *In vitro* transcription-translation (IVTT) system for synthesizing membrane proteins

In vitro transcription-translation (IVTT) systems consist of the components necessary for transcription and the translation mostly from cell lysates thus enabling the *in vitro* synthesis of various target proteins in the test tube [6]. The IVTT system produces MPs independent from the requirements of living cells to maintain alive, therefore, overcomes the limitations of conventional cellular expression systems. In general, MPs require hydrophobic environments to fold and exhibit their function, which can easily be provided by adding liposomes, nanodiscs or detergents to the IVTT system. In addition, protein synthesis using the IVTT system can be performed in various reaction scale including that in smaller volumes (less than 50 μL) compared to traditional method and thus multiple reactions can be performed in parallel with short reaction times (typically less than few hours) [7].

The IVTT system which is currently used is mostly based on *E. coli* cell-extracts and thus derived from prokaryote, while those derive from eukaryote are also available: from wheat germ, rabbit reticulocyte or *Spodoptera frugiperda* cell lines. Furthermore, systems based on Chinese hamster ovary cells, mouse embryonic fibroblasts or HeLa cell lines are also available [4]. All of the aforementioned IVTT systems are derived from living cell lysate, where all components included in the system are not defined. A reconstituted IVTT system, termed the PURE system, is the only reconstituted IVTT system where components required for *E. coli* protein synthesis are highly purified individually and reconstituted in a test tube to carry out the reaction. The reconstituted IVTT system consists of enzymes such as initiation factors, elongation factors, release factors, ribosome recycling factor, 20 aminoacyl-tRNA synthetases, methionyl-tRNA formylase and T7 RNA polymerase. It also contains *E. coli* 70S ribosomes, amino acids, NTPs, *E. coli* tRNA and an energy recycling system [8]. The reconstituted IVTT has an extremely high ability to adjust the constituents. One can remove or add defined components or alter the concentration of any of the components. Furthermore, it has a significantly less nuclease and protease activity. These properties are of advantages when building molecular systems of interest. Indeed, a reconstituted IVTT system has become one of the most popular reconstituted IVTT system used for various application including paper-based biosensor construction [9], artificial cell synthesis [10], and even for discovering peptide drugs. As with other IVTT systems, MPs synthesized with a reconstituted IVTT system required lipid bilayer vehicle to fold and exhibit function. The traditional lipid bilayer set up including proteoliposomes and planner membrane require skilled operators. Besides, the large amount of MPs and lipids are needed for each experiment, which is not favourable and costly.

1-3 Droplet interface bilayer (DIB) for characterizing membrane proteins

The membrane of the living cell is a sophisticated environment, and MPs are located in this complex environment. When isolating MPs from the cells for characterization, they must be placed in an appropriate environment mimicking the cell membrane. Reconstituting the MPs in the form of artificial cellular membrane is one of the most popular strategies to achieve this, where every constituent element can be altered and adjusted. To characterize MPs *in vitro,* one of the most popular strategy is to purify MPs from the cells in the presence of detergents before bringing them to an artificial membrane, and then reconstitute into lipid bilayer such as liposomes, planar bilayer membrane, nanodiscs or bicelles.

A newer developed method is the Droplet Interface Bilayer (DIB) [11]. Pioneer works by the groups of Prof. Baylay [12] and Prof. Takeuchi [13], independently showed that aqueous droplet submerged below a phospholipid dissolved oil mixture will be surrounded by the lipid generating a lipid monolayer around the aqueous droplet. And, once the droplets are brought into contact, the oil between the monolayers is displaced and lipid bilayer will be created. MPs provided within one or both of the droplets will become incorporated into the DIB [14]. DIB approach is one of the simplest ways of forming stable bilayers where various proteins can be incorporated. DIBs have several advantages for the study of MPs; such as smaller amounts of protein are required. The ‘‘lipid-out’’ strategy of forming DIBs are ordinarily used. This primary technique wherever uses lipids dissolved within the oil section. Before contacting the droplets to make bilayer, approximately thirty min is

required for incubation step. The explication of this incubation time is the interval of time needed for monolayer formation [14].

While, DIB is a strategy to easily prepare lipid bilayer, not many MPs have been characterized using this method. Most researchers use α-hemolysin (AH) from *Staphylococcus aureus* as a model protein to demonstrate the DIB formation, while ion channel KcsA has also been studied [15]. One of the reasons that DIB is not used widely is partly because the function of membrane protein in DIB approach has been mostly evaluated only by electrical measurement that requires skilled techniques and limited to channels and pore forming proteins. DIB's potential is restricted mostly by the instability of DIB when localizing the MPs at the DIB and also during functional measurement. [16] Supplying the detergent dissolved MPs prevent the aggregation of MPs but also destroys the DIB. [16] Most of the MPs are thus supplied by adding proteoliposomes inside the w/o droplet and wait for spontaneous fusion to the DIB, which is a very time consuming process. Alternatively, previous studies showed an attempt to supply the MPs directly to the DIB by creating the w/o droplets using IVTT system, however, failed in making stabilized droplet consist of IVTT system. 30 min incubation was required before droplets were contacted, or else fused. [16,17,18,19]

1-4 Objective of this study

As described above, MPs have been hardly used in biotechnology applications because of the difficulty in isolation and purification of functional MPs by the conventional techniques. This study aims to develop a platform to study the properties of membrane proteins by encapsulating IVTT system (the PURE system) inside DIB, thereby enabling

the analysis of MPs easier than previous methods. However, it has been reported that the stability of the DIB was lowered significantly when the DIB was prepared with the droplet consist of an IVTT system. To overcome the problem of unstable DIB made of an IVTT system, I have developed an easy-to-use microchip with a protocol that stabilizes the DIB. Additionally, fluorescence-based functional assay was used, in order to simplify the complexity of detection method, an electrical impedance spectroscopy measurement, that is the most commonly used with the DIB approach. Using this system, I successfully synthesized AH pore-forming toxin and EmrE, a multidrug transporter from *E. coli*, inside the droplet, both localized at the DIB in their functional form. In addition, for the first time I quantified the amount of MPs, *i.e.*, AH and EmrE at the DIB supplied by a reconstituted IVTT system. I believe that this system could be a starting point for the development of a membrane protein-based biosensors.

In Chapter 2, I described about optimizing an experimental condition to create stable DIB prepared by droplets consist of a reconstituted IVTT system by altering the phospholipid dissolved solution and the chamber shape to place the water-in-oil droplet. Then, I described about the usage of the developed DIB system for synthesizing, characterizing and quantifying**,** a pore forming protein from *Staphylococcus aureus*. In Chapter 3, I described about using the developed DIB system for synthesizing, characterizing and quantifying EmrE**,** a multidrug transporter from *E. coli*. Finally, in Chapter 4, I summarized the result and discuss the future aspect of supplying MPs with a reconstituted IVTT system to the DIB.

Chapter 2 Quantifying and characterizing α-hemolysin synthesized using IVTT system localized at DIB

2-1 Introduction

DIB approach is a simple way of forming stable lipid bilayer where various membrane proteins can be incorporated. One of the important requirements for DIB formation is that two water-in-oil (w/o) droplets must come into contact without merging. The temperature and the composition of the oil phase has been reported to influence the lipid behaviour at a droplet interface. [20] The lipid bilayer environment has been reported to affect MPs insertion efficiency and activity. [21] Selection of the suitable temperature and oil phase, result in increasing the formation of stable DIB. The lipid-out technique, during which a typical lipid mixture is present within the oil encompassing all droplets, offers easier preparation of w/o droplets since dispersing lipids in oil avoids the steps necessary for liposome preparation like freeze−thaw, extrusion, or sonication.[22] However, the lipid-out technique has low DIB formation fraction because of poor monolayer formation at the oil/water interface, [17] while, the variations in lipid assembly in the oil phase has never been quantitatively studied to identify the influence of oil phase on the DIBs formation and stability. Multiple works concentrated on stabilization of DIB by focusing on time needed before droplet contact to achieve a level of packing density of detergents that prevent droplet fusion. [23−25] But, only few studies are performed in regard to the w/o dropets made of phospholipid monolayer and DIB formation using them. [26] Several methods developed to stabilize the DIB however, these methods are complicated, costly, and required skills. [27]

DIBs become unstable, the w/o droplets may shrink due to evaporation and eventually detach, or the w/o droplets may increase in size. [28] For functional analysis of MPs including fluorescence detection of membrane transport phenomena, the DIB should be stable during the measurement time. Moreover, chambers design controlled the shape and volume of contacted microdroplets in oil phase. [29–35] The stability of DIB can be simply improved by localizing the contact droplets in chamber. Problem of hardly making stable DIBs raised from the difficulties of handling DIBs. Encapsulated DIB in chamber as a solid substrate are physically restricted w/o droplets, by limiting the movement of contact droplet in chamber [36] and stabilize the contact length of the two w/o droplets. Subsequently, investigation the *in vitro* synthesis of soluble MP in the stabilized DIB made of IVTT system.

Pore-forming toxins is a family of proteins, that are secreted as a soluble monomer which can oligomerise to create pores on the target cells. Protein undergo the membrane-insertion mechanisms serial steps from a soluble monomer, to binding, oligomerisation and penetration into the target plasma membrane. These toxins are secreted by microorganism pathogens and exhibit cytotoxicity for variety of mammalian cells [37]. The pore-forming protein α-hemolysin (AH) is from the gram-positive pathogenic bacterium *Staphylococcus aureus* [37] that is secreted as a soluble, thirty-four kDa monomer (polar structure) [37, 38] that binds to the lipids at the membrane surface; assembles into a heptamer (amphiphilic structure) [38] on the bilayer [8]; and at last generates a nanopores 1.5 nm in diameter with a vestibule of three nm [39]. Assemble of AH heptamer allow bilayer to penetrate molecules smaller than three kDa, and additionally release metabolites and ions, eventually resulting in host cell lysis [8,40, 41, 42, 43].

AH has been used in many previous studies dealing with DIB because of its water soluble property and pore forming activity, which is ideal to investigate the formation of DIB by developed methods or array for high throughput analyses [16, 44, 45] or for forming droplet network [20, 46, 47]. Most of these systems use electrical measurement [15, 16, 45, 48] to show the pore formation that provide few information about transport molecules.

With an electrical measurement using DIB, one can measure the appearance of a pore at single molecular level. The measured current between the two droplets is correlated to the size of the pore, and thus can quantify pore size. On the one hand, if the pore is blocked by for example a large RNA molecule, the current will decrease. This principle was used to detect cocaine in solution at single molecular level by adding an RNA aptamer that specifically bind to cocaine. [49] Their analysis provides a qualitative data, while the fluorescence base analysis provides more quantitative information. For example, one can quantify the number of AH at the DIB. As many of the experimental parameters of the DIB and a reconstituted IVTT system combined approach can altered and adjusted, one can investigate for example the effect of metal ions, lipid composition and additional chemicals.

I can combine the DIB approach and a reconstituted IVTT system to study and characterize AH. In this study, the detection method was based on fluorescence to simplify the complexity of detection method, electrical measurement, that commonly used in DIB approach. Furthermore, fluorescence-based analysis can provide quantitative information different from that of electrical measurement. The *in vitro* fluorescence-

based functional assay works as follows (Fig. 11A); first two w/o droplets were injected inside lipid dissolved oil. By contacting the two w/o droplets, bilayer is formed at the contact area between the two. One droplet contained the reconstituted IVTT system and DNA encoding AH. In this droplet, AH synthesis occurs, and the pore is formed at the DIB. To convert the pore formation to a fluorescence signal, the enzyme and the substrate were separately encapsulated in each droplet. once the protein generates the pore, the substrate (small molecules) diffused to the other droplet. Following that fluorescent signal observed in the other droplet due to the diffusion of small molecules where the enzymatic reaction occurred, resulted in fluorescent product that indicates the synthesis of functional protein.

In this chapter, I investigated the experimental condition for establishing a stable DIB prepared with a reconstituted IVTT system. I firstly investigated whether the efficiency of protein synthesis inside a w/o droplet is different from that in a test tube. I then selected a suitable oil phase for preparing lipid dissolved oil solution that increase the formation and stability of DIB and examined the stability of DIB at 37 °C for 2 h which is a time required for protein synthesis with an IVTT system. After that, I tested the effect of different chamber design on the w/o droplet shape and DIB contact length. Then, I performed the functional assay of AH in the stabilized DIB inside RB2 chamber and quantified the amount of AH heptamers per DIB using fluorescence intensity data. Finally, I changed the lipid composition to improve the insertion of AH at the DIB. Within the present work, I tend to show that MPs synthesized by an IVTT system within a droplet are inserted into the bilayer in its functional form, thereby overcoming several the problems related to previous reconstitution strategies [50].

2-2 Materials and Methods

2-2-1 Preparation of lipid dissolved oil solution

The lipid dissolved oil solution consisted of 1,2-dioleoyl-sn-glycero-3-phosphocholine (DOPC) (Avanti Polar Lipids, AL, USA) as phospholipid and decane (Sigma- Aldrich, MO, USA) or n-hexadecane (Nacalai Tesque, Kyoto, Japan) as oil phase. To prepare lipid dissolved oil solution, lipids dissolved in chloroform was place under vacuum for 2 h at room temperature, followed by dissolving in an oil indicated in the text. The lipid dissolved oil solution could be used at most for a week, and older solution showed decreased fraction of DIB formation (data not shown). Therefore, lipid dissolved oil solutions were used at most for a week after their preparation.

2-2-2 *In vitro* transcription and translation system

I used a reconstituted IVTT system (PURE system) that contains all of the components essential for the transcription and translation. The composition of all the components are described previously [10, 51]. Protein synthesis with a reconstituted IVTT system was performed by mixing 10 nM DNA (PCR product) to the IVTT system supplemented with 0.4 units of RNase inhibitor (RNasin). The reaction was initiated by placing the reaction mixture at 37°C.

PCR products used for protein synthesis were prepared as follows. PCR was performed using plasmids encoding GFP [52, 53] by KOD-plus (TOYOBO, KOD-201) with the primers T7 F (5'-TAATACGACTCACTATAGGG-3') and T7 R (5'-GCTAGTTATTGCTCAGCGG-3'). The PCR product was purified by using a QIA quick PCR purification kit (Qiagen) according to the manufacturer's instructions (Qiagen). The

purity was confirmed by absorbance spectrum and agarose gel electrophoresis. Finally, the DNA concentration of the PCR product was determined by nanodrop.

Real-time PCR machine (Mx3005P, Stratagene) was used for measuring the fluorescence of GFP synthesized by a reconstituted IVTT inside a test tube as well as inside an IVTT droplet in an oil phase. For GFP synthesis in a test tube, 20 µL reaction mixture [a reconstituted IVTT system mixed with 10 nM GFP DNA (PCR product), 0.4 units of RNasin, and 0.04 µM Alexa fluor 647 as a reference dye] was prepared in 0.2 mL tube. For GFP protein synthesis inside w/o droplet, 20 µL of lipid dissolved oil solution [20mg/mL DOPC in a mixture of 10:1 (v/v) hexadecane and decane] was added in 0.2 mL tube followed by an addition of 20 µL mixture of a reconstituted IVTT system [IVTT mixed with 10 nM GFP DNA (PCR product), 0.4 units of RNasin, and 0.04 µM Alexa fluor 647 as a reference dye]. The 0.2 mL tubes were incubated at 37°C for 4 h in real-time PCR machine and the fluorescence was measured every 2 min.

2-2-3 Chamber preparation

Three different chamber designs—flat-bottom (FB), round-bottom V1 (RB1), and round-bottom V2 (RB2)—were prepared, the detailed size is described in Fig. 8. The chambers were fabricated using an acrylic plate using a micromilling machine (MM-100, Modia Systems) with dimensions as indicated in the results section and the resulting droplet interface stability was assessed by measuring the contact length of the two droplets over time via microscopy (Fig. 8 and Fig. 9).

2-2-4 α-hemolysin synthesized by IVTT system and its characterization

For AH synthesis, 10 nM AH encoding DNA (PCR product) was added to an IVTT supplemented with 0.4 units of RNasin. Then incubate at 37 °C to initiate the reaction.

PCR products were prepared and purified as described above except that the plasmid used for amplification was encoding AH [37,38]. Finally, I confirmed the purity with an agarose gel electrophoresis (Fig. 1) and determine the concentration of the PCR product by nanodrop.

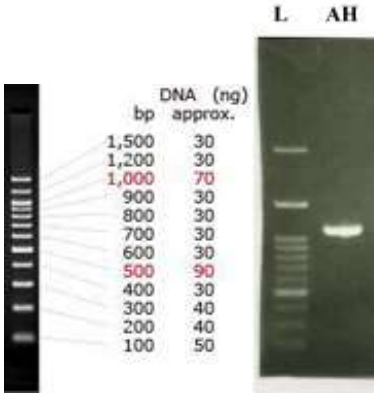

Fig. 1: Gel electrophoresis for the PCR product. I confirmed the purity of PCR product by performing gel electrophoresis. The length of the product was as expected (1024 bp). Nacalai DNA ladder broad range 100 bp was used as a DNA marker.

2-2-5 Functional assay of AH

I performed the functional assay of AH with a strategy as shown in Fig. 11A except that the RB2 chamber was used. RB2 chamber was filled with 14 µL of lipid dissolved oil solution [20 mg/mL DOPC in a mixture of 10:1 (v/v) hexadecane and decane], and two aqueous droplets of 3.5 µL were added to each position of RB2 chamber. For the assay, left droplet contained (a reconstituted IVTT, 10 nM AH DNA (PCR product), 200 µM FDGlcU (1 kDa)—a substrate of β-glucuronidase (GUS), 0.4 units RNasin, 2 µM T7 polymerase) while right droplet contained (a reconstituted IVTT, 100 nM GUS enzyme, 0.4 units RNasin, 1 µM ovalbumin conjugated to Alexa-Fluor 647 (OA647) (45 kDa)). After formation of the two w/o droplets, the chambers were incubated on thermoplate at

37 °C for 2 h, followed by an incubation at 25 ºC. Image recording every hour under fluorescence microscopy.

2-2-6 Data processing

Images were analysed using ImageJ to quantify the mean fluorescence intensity of each droplet. Background fluorescence, where the fluorescent compound is not present, was subtracted from the mean fluorescence intensity of the DIB at each time point, followed by subtracting the fluorescence intensity at time zero. To calculate the concentration of hydrolyzed FDGlcU from the fluorescence of the droplet, FDGlcU was hydrolysed completely by incubating with GUS for overnight at 37 ºC. The hydrolysed FDGlcU was then diluted and the correlation between hydrolysed FDGlcU and the fluorescence intensity of the droplet was plotted (Fig.9). This standard curve was used to calculate the amount of FDGlcU which flowed into the adjacent droplet.

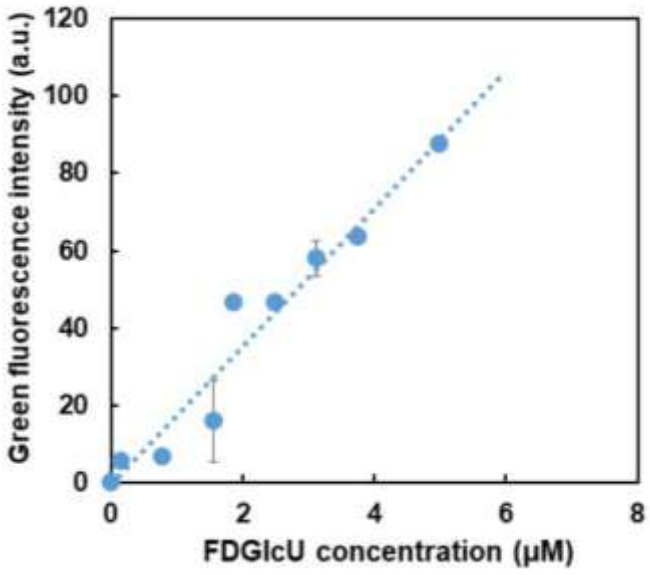

Fig. 2: Correlation between the hydrolysed FDGlcU concentration and green fluorescence intensity inside the droplet. A 200 μM FDGlcU concentration was hydrolysed by GUS to completion, and the resulting solution was diluted with a reconstituted IVTT system to the

concentration indicated on the horizontal axis. The 3.5 μL w/o droplets were prepared and observed under a microscope, and the fluorescence intensity was measured. The dashed line indicates the linear trendline.

2-3 Results

2-3-1 Comparing GFP synthesis by a reconstituted IVTT inside a test tube and inside w/o droplet with different lipid dissolved oil solution

Adjusting the oil phase may improve the stability of the DIB, while it should not affect the protein synthesis efficiency using a reconstituted IVTT system. Firstly, I thus tested the ability for synthesizing a functional protein using an IVTT system inside w/o droplet and compared the efficiency with that inside a test tube (Fig. 3). Secondly, I checked the effect of different oil phases on the efficiency of protein synthesis using an IVTT system inside w/o droplet.

I used GFP as a reporter gene. DNA encoding GFP was added to an IVTT system and incubated at 37 °C, and the green fluorescence was measured. Fluorescence intensity increased in both IVTT system in the test tube and inside the w/o droplet where the water phase consists of an IVTT system, indicating the synthesis of GFP in both conditions (Fig. 4). No fluorescence intensity was observed in the absence of DNA (no DNA).The time course of GFP fluorescence inside a w/o droplet and the test tube were almost the same (Fig, 2), indicating that the presence of the lipid dissolved oil phase (20 mg/mL DOPC in a mixture of 10:1 (v/v) hexadecane and decane) had little effect on the protein synthesis.

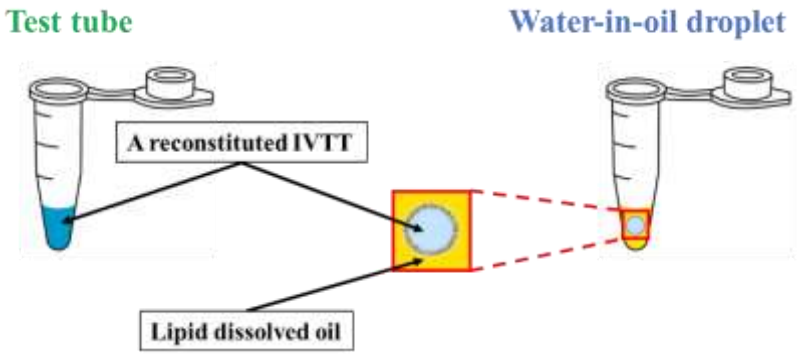

Fig. 3: Schematic of protein synthesis using an IVTT inside a w/o droplet and a test tube. GFP synthesis was performed by an IVTT inside a test tube (left tube) or inside a w/o droplet (right tube). Then different lipid dissolved oil solution 20 mg/mL DOPC in mixture of 10:1 (v/v) hexadecane and decane, 20 mg/mL DOPC in hexadecane, or 20 mg/mL DOPC in decane were used as an oil phase.

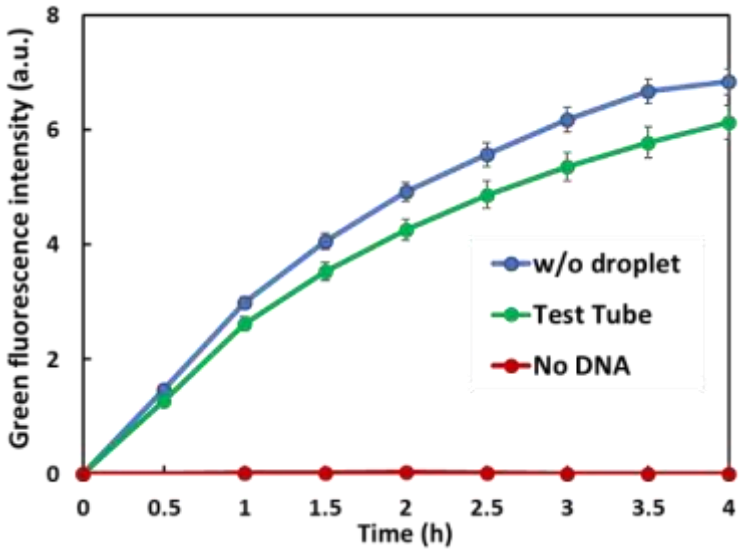

Fig. 4: GFP protein synthesis by IVTT inside the tube or w/o droplet. Mean GFP fluorescence (n = 3) are shown. Error bars indicate the standard error of measurement (s.e.m.). All fluorescence intensities were normalized by dividing the GFP fluorescence by AlexaFluor 647 fluorescence, added at constant concentration in all tubes to normalize the difference among the tubes. Reaction was performed at 37 ºC and GFP fluorescence was measured during the protein synthesis every 30 min.

I then performed GFP synthesis by a reconstituted IVTT system inside a droplet with three different lipid dissolved oil solutions: 20 mg/mL DOPC in a mixture of 10:1 (v/v) hexadecane and decane, 20 mg/mL DOPC in hexadecane, or 20 mg/mL DOPC in decane. These three oil phases are commonly used in forming DIBs [54, 55]. In brief, 20 µL of an IVTT system containing 10 nM GFP DNA was added to a lipid dissolved oil solution and incubated at 37 °C, and the GFP fluorescence was measured every 30 min (Fig. 5).

The GFP fluorescence increased inside droplet in all w/o droplets tested indicating the synthesis of GFP protein. No fluorescence intensity observed in the absence of GFP encoding DNA (no DNA). In addition, GFP fluorescence increased similarly inside w/o droplet in different oils, indicating that oil phase tested hardly affect the protein synthesis inside the w/o droplet.

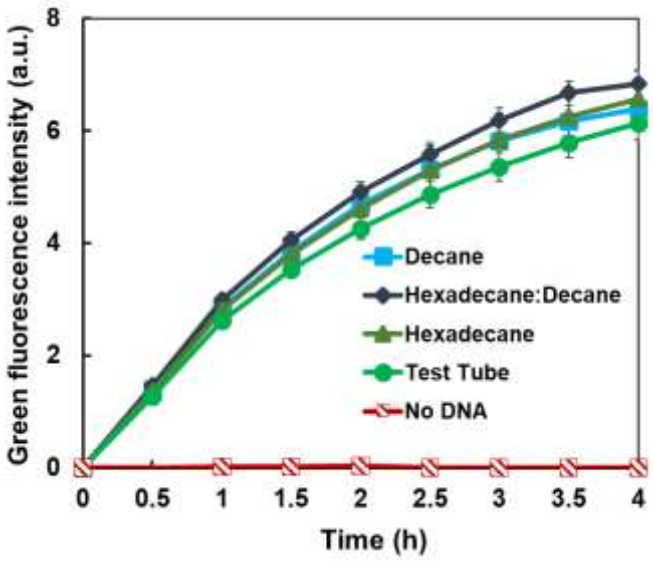

Fig. 5: GFP synthesis by an IVTT inside w/o droplet in three different oil phases. Mean GFP fluorescence (n = 3) are shown. Error bars indicate the s.e.m All fluorescence intensities were normalized by dividing the GFP fluorescence by AlexaFluor 647 fluorescence, added at constant concentration in all

tubes to normalize the difference among the tubes.

2-3-2 DIB formation fraction and its stability at 37 °C

To generate a DIB with droplets made of a reconstituted IVTT system that can be maintained for a few hours, a time required for protein synthesis, I first investigated the effect of lipid dissolved oil phase on the stability of the DIB. The fraction of DIB formation, defined as two w/o droplets contact at room temperature without fusion, was measured (Fig. 6). The experiment was performed at room temperature with two 3.5 µL droplets made of an IVTT system, one droplet with 20 µM calcein (green fluorescent dye) incorporated to confirm the intact droplet interface. I used a flat chamber made of acrylic plate (Fig. 8, top left schematic), and a standard micropipette for droplet preparation. Unlike previous studies, in which the droplets required incubation time before contact about 5–20 min [56, 57], the two droplets were contacted immediately. I analysed the formation fraction of DIB at room temperature for three different lipid dissolved oil solution 20 mg/mL DOPC in mixture of 10:1 (v/v) hexadecane and decane, 20 mg/mL DOPC in hexadecane, and 20 mg/mL DOPC in decane. These three were used as they all showed no inhibitory effect on the GFP synthesis (Fig. 5). As shown in Fig. 6C, DIB preparation was defined successful when calcein was maintained in one of the droplet after two droplets were contacted, while the failure was defined when the two droplets fused which can be seen as the calcein present in both droplets.

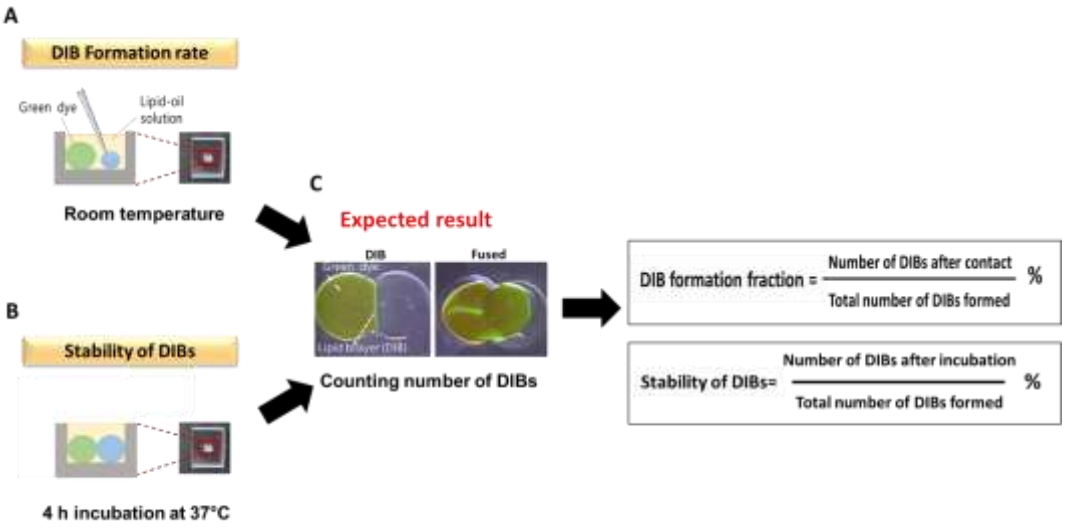

Fig. 6: Schematic of how DIB formation fraction and its stability was measured. (A) Schematic of the quantification of the DIB formation fration. Chamber filled was first filled with lipid dissolved oil solution, and a droplet containing a reconstituted IVTT with 20 μM calcein (green dye) was loaded. Then, the second droplet that contained only an IVTT solution (blue droplet) was loaded, and the two droplets were made to contact. DIB formation fraction is the number of DIBs remained after the contact. (B) The stability of DIBs is the number of DIBs remained after incubation at 37 °C for 4 h on a thermoplate. (C) Two representative pictures of expected results. Left shows the picture of successful DIB formation and stable DIB. Calcein (green dye) is occluded in the left droplet. Right shows the picture of failure in DIB formation and unstable DIB. Two contact droplets fused due to the rupture of DIB and spread of calcein occurs in the two droplets. The DIB formation fraction and stability of DIBs calculated by using these equations.

The stability of DIB was investigated, the fraction of the DIB remaining after incubation at 37 °C for 4 h was measured (Fig. 6B). Measuring the stability of the DIBs at 37 °C since the initiation of protein synthesis via an IVTT system required this temperature. Similarly, as shown in Fig. 6B, stable DIB was defined by the DIB maintained, that is calcein maintained in one of the droplet after 4 h at 37 ºC, while the unstable DIB was defined by the two droplets fused, that is calcein spreads in both droplets during 4 h at 37 ºC incubation.

The highest DIBs formation fraction, and the stability of DIB was obtained by using 20 mg/mL DOPC in a mixture of 10:1 (v/v) hexadecane and decane (Fig. 7). Based on these findings, I decided to use a 20 mg/mL DOPC in mixture of 10:1 (v/v) hexadecane to decane for all subsequent experiments. I will discuss the mechanism of why the mixture showed the best performance in the mixture of 10:1 (v/v) hexadecane to decane.

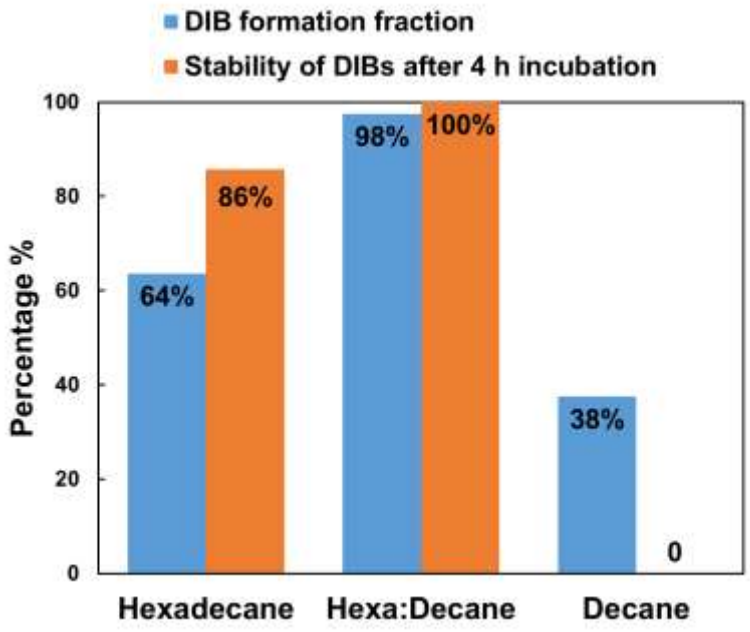

Fig. 7: The DIB formation fraction and its stability. Two features were investigated with different lipid-oil solution [20 mg/mL DOPC in hexadecane (n = 11), 20 mg/mL DOPC in mixture of 10:1 (v/v) hexadecane and decane (n = 40), and DOPC in decane (n = 9)]. Details are described in the text.

2-3-3 Effect of chamber design on contact length between two droplets

During the stability measurements described above, I realized that the droplets changed shape and positions within the flat chambers during incubation, which likely affected the contact area of the droplets, which is not suited for quantitative experiments. I thus

thought this problem might be solved by varying the chamber shape and design. For that reason, three different chambers were designed and prepared—flat-bottom (FB), round-bottom V1 (RB1), and round-bottom V2 (RB2) (Fig. 8). The chambers were fabricated using an acrylic plate using a micromilling machine with dimensions as indicated in Fig. 8. The contact length of the resulting droplet interface was measured via microscopy to evaluate the stability (Fig. 8 and Fig.7). In brief, two IVTT droplets of volume 3.5 µL were prepared without adding template DNA submerged in 10: 1 (v/v) hexadecane to decane containing 20 mg/mL DOPC and incubated at 37 °C, and the contact length was measured hourly (Fig. 8).

A decrease in contact length during the incubation with high variation among the samples has been observed with the FB and RB1 chambers. In contrast, the RB2 chamber showed suppressed variation among the samples (Fig. 8). Notably, no droplet fusion occurred, regardless of the chamber design used for the experiment. These results indiacate that the chamber design affect the contact length between the w/o droplet, and RB2 showed the best results since RB2 design restricted the w/o droplet movement (Fig.7). As will be shown later, the chamber shape affected the results the functional characterization of a MPs (Fig. 12).

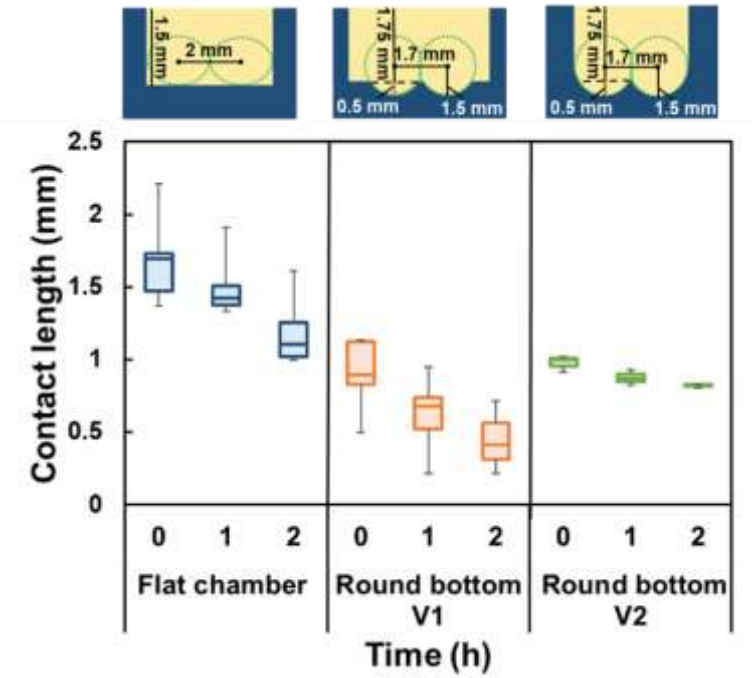

Fig. 8: Chamber design affects the contact length between two droplets over time. The chambers were fabricated using an acrylic plate using a micromilling machine. The box plot shows that the variation in contact length of the flat (n = 9), the round-bottom V1 chamber (n = 9), and the round-bottom V2 chamber (RB2) (n = 9). Contact length was measured as shown in Fig. 9.

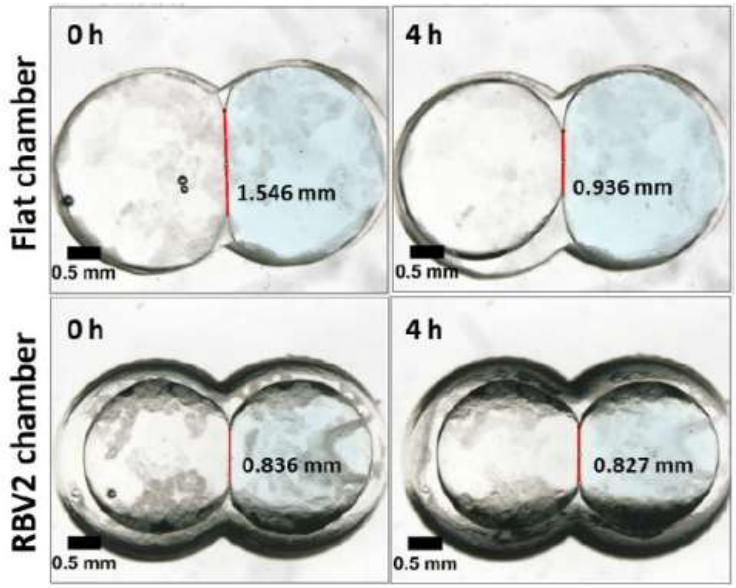

Fig. 9: Contact length measurement. Representative images of the DIB at 0 h and 4h in the FB (flat-bottom chamber) and RB2 (round-bottom V2) chamber, respectively. The contact length between the droplets is indicated by the red line, and the measured length is indicated next to it. Scale bar represents 0.5 mm. The images were analysed by ImageJ.

2-3-4 Functional assay of AH by using fluorescence substances.

I aimed to test the synthesis of functional membrane protein by an IVTT system inside DIBs. Here, I used AH as a model protein (Fig. 10), whose function was analysed by observing the fluorescence intensity of the droplet increasing by time (Fig. 11A). Generally, AH synthesize in form of a soluble monomer, then that monomers binds to phospholipids and oligomerized into heptamerizes on the bilayer to generate nanopores, where molecules smaller than approximately 3 kDa can pass though. A substrate of β-glucuronidase (GUS), FDGlcU which has molecular weight about (1 kDa), and a DNA template encoding AH have been added to the left 3.5 µL IVTT droplet. In the other side, the right IVTT droplet contained GUS enzyme and ovalbumin conjugated to AlexaFluor647 (OA647) which has molecular weight about (45 kDa). Diffusion of FDGlcU from left droplet into right droplet, as AH synthesized in the left droplet. Since right droplet contained GUS, FDGlcU was hydrolyzed and consequence green fluorescence result. As shown in Fig. 11B, neither the droplet shape nor the droplet location was changed during the incubation time. Notably, only the observation of green fluorescence dedicated with the left droplet that contained AH DNA. Moreover, the red fluorescence dye (OA647) (45 kDa) could not pass through the nanopore to the left droplet due to its high molecular weight. These results confirm the formation of AH-specific nanopores.

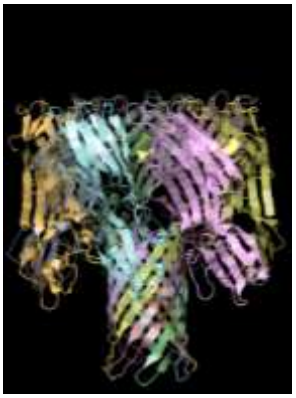

Fig. 10: Three-dimensional structure of AH. Each monomer units are shown in different color. AH is expressed as a soluble monomer and assemble into heptamer on the membrane.

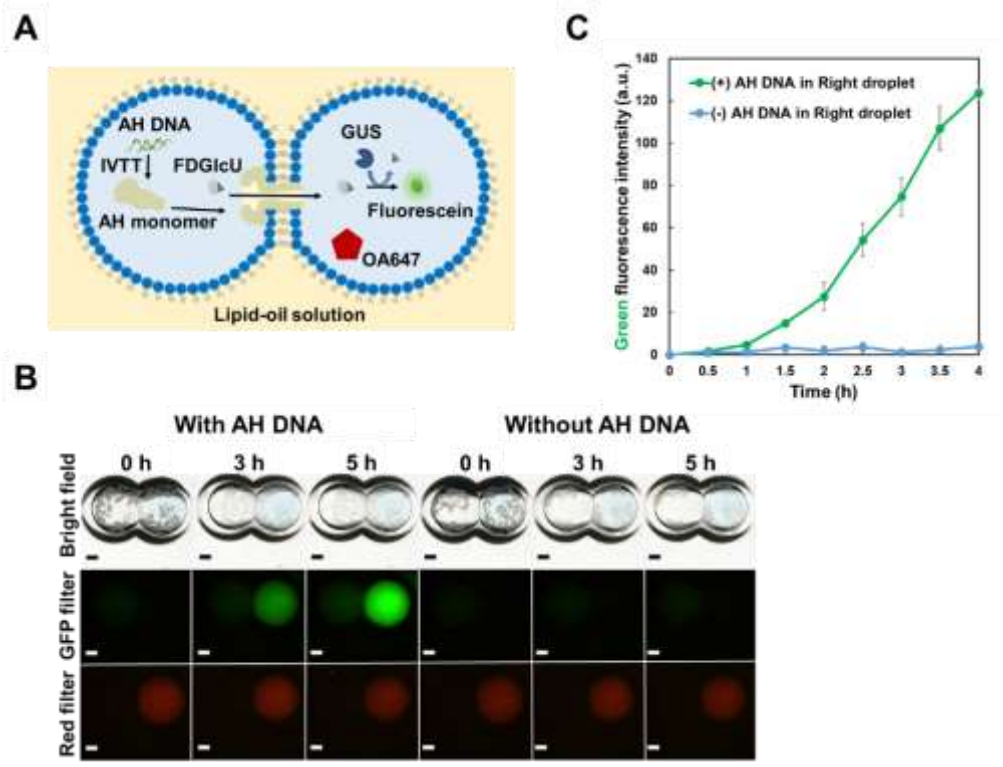

Fig. 11: Functional synthesis of AH. (A) Schematic of the fluorescence-based functional assay of AH using DIB. (B) Representative image of fluorescence-based functional assay. (C) Time course of green fluorescence intensity (n = 3). Error bars indicate the s.e.m. The scale bar is 0.5 mm. The chamber was incubated at 37 °C for 2 h, followed by incubation at 25 °C. The time indicated is the total incubation time at 37 °C and 25 °C.

2-3-5 Comparing the effect of chamber design on the fluorescence flux through AH pores

As the chamber design influencing the contact area of the two droplets. I found that the chamber shape, also affects the functional assay of AH. In brief, the AH synthesis was performed using two different chambers, FB and RB2, and the change in the fluorescence intensity was measured. As shown in Fig. 12, it is clear that RB2 show stronger fluorescence indicating that RB2 chamber creates more lipid bilayer area than the FB chamber. From these observations, the results suggest that RB2 chamber is better than the others when creating DIB using a reconstituted IVTT system.

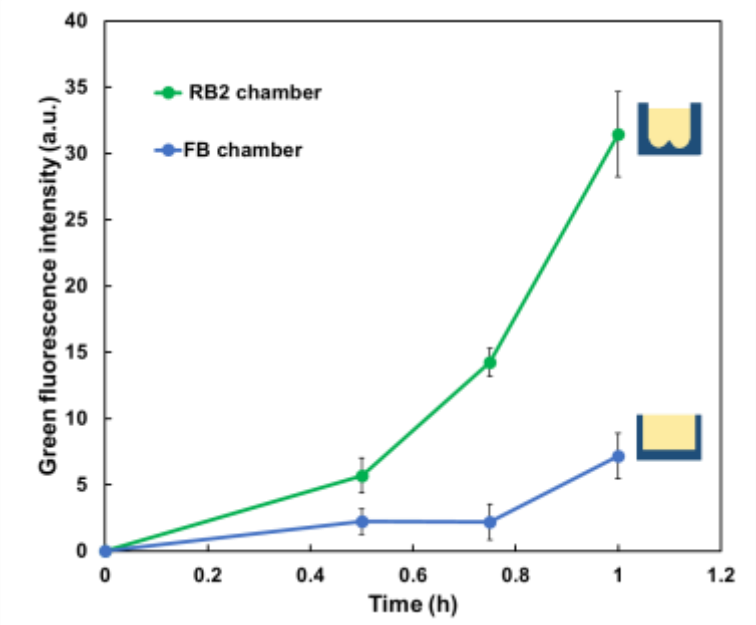

Fig. 12: FDGlcU hydrolysis by AH synthesized in RB2 or FB chamber. Data are the mean of 3 samples and error bars indicate s.e.m.

2-3-6 Quantifying the amount of α-hemolysin at the DIB

I then aimed to quantify the amount of AH at the DIB from the data shown in Fig. 11B. Firstly, I measured and quantified the green fluorescence intensities of the droplets (Fig. 11C, green) and observed a concave curve for the first 2 h in the presence of AH encoding DNA, followed by a nearly linear increase, indicating that the number of pores was not significantly increased after 2 h. No increase in green fluorescence was observed in the absence of AH encoding DNA (Fig. 11C, blue), indicating that the increase in the green fluorescence above is due to the presence of AH at the DIB.

After that, the amount of AH localized within the DIB has been calculated. The values of green fluorescence were converted from fluorescence intensity to number of FDGlcU molecules by using a correlation between the green fluorescence intensity and the fully hydrolysed FDGlcU concentration (Fig.9). From this the value *n* calculated as (8.2×10^{-12} mol h^{-1} = 3.5 μL x 2.35 $\mu M h^{-1}$), that represented the amount of FDGlcU that diffused from the left to the right droplet in 1 h. The flow of FDGlcU can be written using Fick's first law as:

$$J = -D\,dC/dx = -D\,((C_R - C_L)/L) \quad (1)$$

where *J* is the flux of FDGlcU and D is the diffusion constant of FDGlcU. As the diffusion constant of FDGlcU is not reported, for that difluorofluorescein value has been used $D = 1.44 \times 10^{-6}$ m^2 h^{-1}. [58] C_R and C_L represent FDGlcU concentrations in the right and left droplets, respectively. From the result, only a small fraction of FDGlcU diffused into the adjacent droplet, with a maximum concentration of hydrolysed FDGlcU of approximately

7 µM in the right droplet. Thus, the difference in concentrations could be approximated as 200 µM, which was the initial concentration of FDGlcU. *L* represents the distance through which the molecules pass, which corresponded to the thickness of AH in this case, defined as 3 x10^{-9} m [59]. From these values, I obtained *J* = 96 mol m^{-2} h^{-1}. *J* can also be expressed as:

$$J = n/A_T \qquad (2)$$

where A_T is the total area through which FDGlcU molecules pass in the AH pores. From eqn (2), and given that n and *J* were calculated, I obtained A_T= 8.5 x 10^{-14} m^2 (= 8.2 x 10^{-12} (mol h^1)/96 (mol m^{-2} h^{-1})). The number of AH nanopores inserted into the bilayer (N_{pore}) can be calculated as below:

$$N_{pore} = A_T / A_{pore} \qquad (3)$$

where A_{pore} = 1.8 x 10^{-18} m^2 is the pore size of individual AH molecules [67]. Finally, I obtained N_{pore} = 4.8 x 10^4 heptamers per DIB. I assume that the protein synthesized inside the droplets using IVTT is in distinguishable from that synthesized in a test tube (Fig. 4). I therefore quantified the number of heptameric AH (N_{AH}) in a 3.5 µL droplet by labelling AH using [^{35}S]-methioine, SDS-PAGE, and autoradiography (Fig. 13), wherein N_{AH} = 2.0 x 10^{12} heptamers. Finally, the fraction of AH inserted into the bilayer was determined to be 2.4 x 10^{-6} % of the total amount of AH synthesized. This also corresponds to a density of 0.049 AH $µm^{-2}$, where the contact area of the DIB was calculated using the contact length (Fig. 9) as the diameter. Although only a small fraction of AH inserted into the DIB, this amount was sufficient to exhibit detectable function.

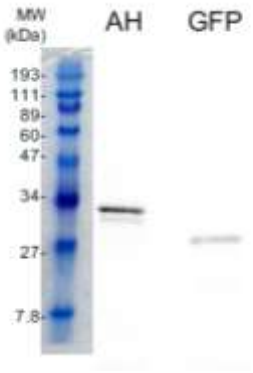

Fig. 13: Quantifying the amount of AH synthesized using IVTT. AH synthesis using a reconstituted IVTT was performed in the presence of [^{35}S]-methionine, with an AH DNA concentration of 10 nM at 37 °C for 2 h. The total amount of AH synthesized was quantified from SDS-PAGE, followed by autoradiography. GFP was synthesized as a control.

2-3-7 Effect of lipid dissolved oil solution on the fluroscence flux

Because the constituents of the system can be altered easily, I then aimed to investigate how can increase the amount of AH inserted at the DIB by altering components, such as the lipid composition. I tested the addition of sphingomyelin (SM) and cholesterol (CHO), which cluster together to form membrane structure aid AH to insert. I first tested the effect of adding SM and CHO mixture on the stability of DIB. The stability of DIB was measured as described in Figs. 4 and 5. In brief, three different lipid dissolved oils were prepared: (1) 20 mg/mL DOPC, 2 mg/mL CHO, 1 mg/mL SM, (2) 20 mg/mL DOPC, 4 mg/mL Cholesterol, 2 mg/mL SM, (3) 20 mg/mL DOPC, 6 mg/mL Cholesterol, 3 mg/mL SM. Among the three, the 3 mix oil with composition (20 mg/mL DOPC, 4 mg/mL Cholesterol, 2 mg/mL SM) showed the best results (Fig. 14A). I therefore chose this oil solution for the further experiments.

Next, AH function was measured based on the increase in the fluorescence signal. Experiment was performed essential as described in Fig. 11C, except that the oil solution was changed. By measuring the increase in the fluorescence, I found that that 3-mix oil showed about 2-fold increase in the fluorescence compare with DOPC alone. To confirm that the addition of SM and CHO has increased the number of functional AH localized at the DIB, I calculated the amount of AH based on Fick's first law as described above. In case of 20 mg/mL DOPC, I found that only N_{pore} = 3.3 x 10^4 heptamers per DIB. By altering the lipid composition to 20 mg/mL DOPC, 4 mg/mL Cholesterol, 2 mg/mL SM, I obtained about 2-fold increasing in the amount of AH localized at the DIB (N_{pore} = 7.8 x 10^4 heptamers per DIB). It is important to note that more parameters can be alter such as the component of the IVTT system to further increase the amount of AH at the DIB.

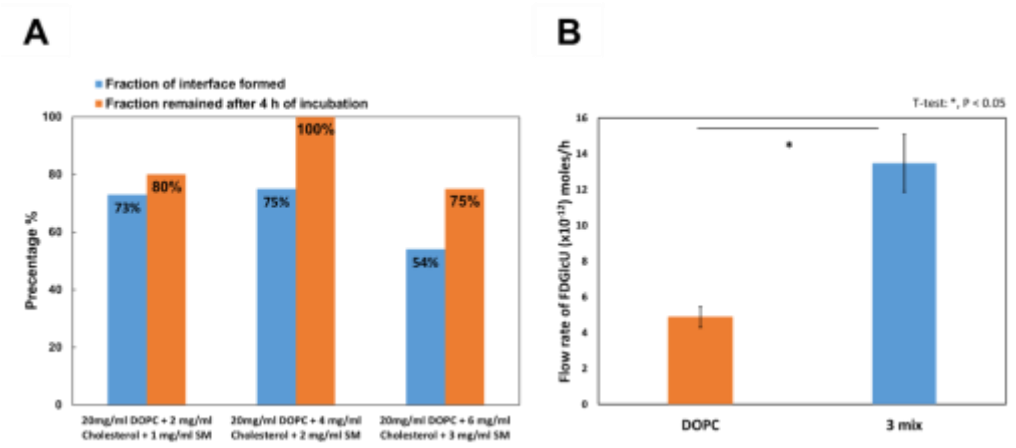

Fig. 14: Effect of adding sphingomyelin (SM) and cholesterol (CHO) to lipid dissolved oil solution. (A) The DIB formation fraction and its stability in the presence of different concentration of SM and CHO. (B) 3 mix lipid dissolved oil solution consist of 20 mg/mL DOPC, 2 mg/mL SM, and 4 mg/mL CHO. The 3-mix oil solution (blue line) showed about 2-fold increase in the flow rate of FDGlcU than that with DOPC (orange line).

2-4 Discussion

I found that a reconsituted IVTT has an ability to synthesize GFP inside w/o droplet with similar efficiency when compared to that in the test tube (Fig. 4). Even using different phosopholipid dissolved oil solution, GFP synthesis inside a w/o droplet was not affected (Fig. 5). In contrast, phosopholipid dissolved oil solution showed a detectable effect on the DIB formation (Fig.5). To achieve the highest DIB formation efficiency and stability, a 20 mg/mL (DOPC) in mixture of 10:1 (v/v) hexadecane to decane was found to be effective, while the detailed mechanism remains unclear. Additionally, I found that the chamber design has an effect on the contact length of the DIB, and that RB2, which was designed to stabilize the location of the droplet, showed the highest stability among those which have been tested (Fig. 8 and Fig.7). The *in vitro* fluorescence-based functional assay with AH has been established and the function of AH confirmed by the diffusion of small molecule (FDGlcU) through AH nanopore, then FDGlcU hydrolysed by GUS enzyme (Fig. 11). Then the percentage of AH at the bilayer to the total AH synthesized has been quantified and obtained N_{pore} = 4.8 x 10^4 heptamers per DIB, whereas the fraction of AH incorporated into the bilayer was determined to be 2.4 x 10^{-6} % of the total amount of AH synthesized. As *in vitro* functional assay is controllable, this feature provides a possibility to investigate various parameter affecting the AH insertion and consequence the fluorescence flux. As a demonstration, the effect of lipid composition on AH has been investigated. I confirmed that change lipid bilayer composition into 20 mg/mL DOPC, 4 mg/mL CHO, 2 mg/mL SM from DOPC alone increased the insertion of AH into bilayer. It has been reported that the presence of SM, CHO, and PC in membrane aid in MP associated to the membrane and mediate quick pore forming. [16] This lipid dissolved oil showed the highest DIB formation fraction and stability and

significantly 2-fold increase in the amount of AH inserted at DIB compare with 20 mg/mL DOPC (Fig. 14).

I showed that protein synthesis using a reconstituted IVTT in lipid dissolved oil solution occurs similarly to that in the test tube. There has been a great interest in comparing the reaction efficiency in confined volume. For example, the comparison of GFP synthesis using a reconstituted IVTT in femtoliter sized liposome or microchamber and that in the test tube was compared [60, 61]. The results showed that GFP synthesis using a reconstituted IVTT occurs similarly both in liposomes and in microchambers. These results emphasizing the efficiency of IVTT system in protein synthesis regardless the surface to volume ratio and the synthesis occurred in liposome, microchamber, or droplet. While there is other report showing that confined reaction space increases the GFP synthesis [56, 62], the w/o droplet here has a volume of 20 μL and thus has a higher surface-to-volume ratio compared to 3.5 fL container. Therefore, it is reasonable to think that the oil phase has little effect on the reconstituted IVTT system.

I reported that 20 mg/mL (DOPC) in mixture of 10:1 (v/v) hexadecane to decane resulted in the highest DIB formation (98 %), and also 100 % of the DIB remained after a 4 h incubation at 37 °C. The mechanism of high stability with a mixture of 10:1 (v/v) hexadecane to decane remains unclear. Previous papers reported that oil phase should have lower viscosity and high melting point, thus mostly hexadecane [54], decane[63], and mixture of hexadecane and decane[14, 16, 64] are chosen. When the water droplet made inside an oil phase, a force is generated: namely interfacial tension, at the OW interface between water and oil molecules due to the relative strengths of attractive and repulsive

Van Der Waals forces. Self-assemble of lipid at the OW interface decreases this bilayer tension. [26] DIBs formed in decane oil have higher bilayer tension than that in hexadecane. The higher tension promote phospholipid assemble at OW interface. A thick bilayer formed in decane indicates the presence of oil between the bilayer, while hexadecane is known to reduce the oil in between. [64] Therefore, mixture of hexadecane and decane might promote the formation of DIB and reduce the oil in bilayer, resulting in relaxed interface and enhance the stability of the bilayer. I also observed the evaporation of decane oil during the incubation at 37 °C, that clarified the low DIBs formation of w/o droplet in decane oil and the fusion of all w/o droplets at 37 °C.

The RB2 chamber suppressed variation among the samples compared with other chamber designs (Fig. 8). Notably, no droplet fusion occurred with RB2: 100 % of DIB was maintained for 2 h. DIB consists of water droplet in oil (liquid-in-liquid). [35] There are three main forces affects the DIB stability: the gravity, the interface tension, and the evaporation. Gravity force could affect the shape of droplet resulting in elliptical or irregular shape that has been observed in flat chamber and RB1 chamber. The RB2 design maintained the spherical shape of the droplet that is not achieved by the flat chamber or RB1 chamber. Moreover, the interface tension of bilayer is affected by the contact angle that is defined as the angle between the bilayer formed. The high variation among DIBs formed in flat chamber resulting from the diverse contact angle since the DIBs in flat chamber are freely moving. RB1 chamber has higher contact angle (90°) than RB2 chamber (60°). By increasing the contact angle, the interface area between the DIBs (contact length) increases, which simultaneously increases the interface tension of the bilayer formed by the high pressure, therefore the probability of vesicle fusion increased.

Additionally, shape of DIBs changed due to evaporation of water from DIB into the oil phase. [64] However, preventing evaporation of DIBs contents and maintain its shape has been applied for all the chambers design, by complete submerging the DIBs in oil phase that isolate the DIBs from air contact. That assent that interface tension force has the main effect on the stability of DIBs.

RB2 chamber designed to limit the droplet movement and located the droplet in specific position, where the round bottom enhanced the spherical shape of the droplet. Moreover, the contact angle (60°) reduced the pressure at the bilayer, avoiding the DIBs fusion.

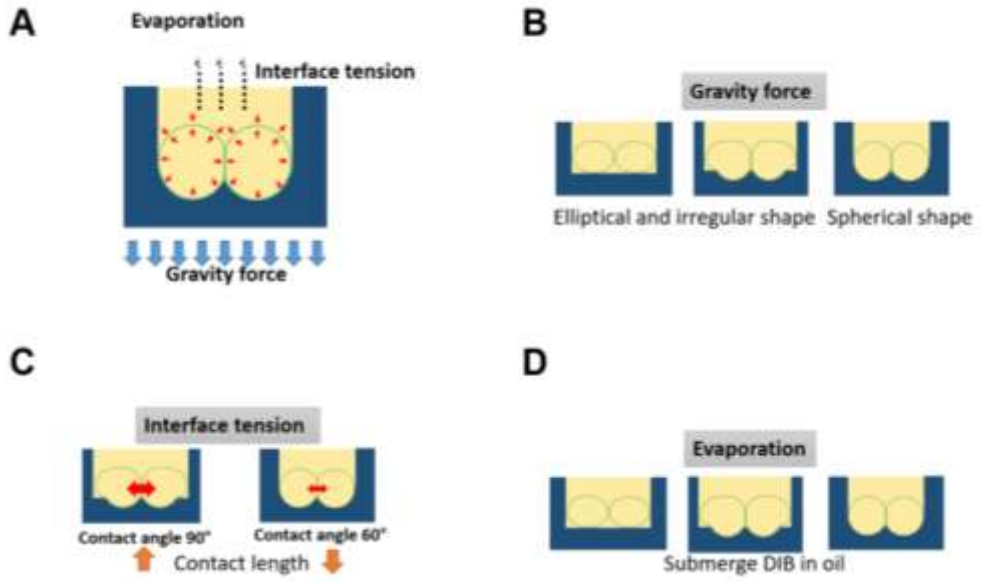

Fig. 15: Forces affecting DIBs stability. (A) Gravity force, interface tension, and evaporation affect the stability of DIBs differently inside each chamber design. (B) Gravity force affect the shape of DIBs. The droplets in FB and RB1 chamber became elliptical and irregular shape while the design of RB2 chamber maintained the spherical shape. (C) Large contact angle result in large contact length at the bilayer area,

increasing the interface tension at the DIBs. (D) Evaporation was avoided by complete submerging the DIBs in oil phase and covering the chamber with a lid.

In vitro fluorescence-based functional assay I developed showed high flexibility, and I indeed succeeded in enhancing the rate of fluorescence intensity by changing the chamber design and lipid composition. The assay can be applied for other MPs. While AH is a unique MP that is expressed as a soluble monomer, most of the MPs aggregate and become insoluble in the absence of a hydrophobic environment. As a next, I tested one of such MPs to verify the ability of the *in vitro* fluorescence-based functional assay.

Chapter 3: Quantifying and characterizing EmrE synthesized using IVTT system localized at DIB

3-1 Introduction

Living cells are affected by cytotoxic compounds that are present in natural environment, while many of them has been observed to have resistance to a large variety of cytotoxic compounds. One of the strategies that organisms have developed is the removal of the cytotoxic substances by transporting them outside of the cells. A wide variety of substrates can be removed, and its concentration is reduced by multidrug transporters, found in bacteria to human, in an energy-dependent manner. Multidrug transporters have been classified into five families based on their properties [65]. Small multidrug resistance proteins (SMR) are one among these 5 superfamilies of transporters, which has a length of around 100 amino acid residues with four transmembrane-helical domains. These proteins are known to eliminate mostly cytotoxic compounds from the cytosol based on a drug/H^+ antiport mechanism. The most extensively studied SMR protein is EmrE, from *E. coli*. [66].

EmrE is a 12-kDa molecule, only one hundred ten residues in length with 4 transmembrane domins that functions as an anti-parallel homodimer (Fig. 16). The transmembrane domain contains only one charged residue (Glu) [67]. The charged residue (Glu) is an important part of the single binding domain that recognized the complete vary of various substrates and exchange between substrates and protons [66]. For each molecule of polyaromatic cation substrate exported by EmrE, there are two protons imported to the inner membrane [68].

Most of previous studies of EmrE characterization used proteins overexpressed and purified from *E.coli* [69, 70, 71, 72]. In addition, the functional assays are mostly done in detergent-solubilized transporter [73, 74], an environment different from that in the cell. Due to difficulties in overexpression and purifying MPs from living cell, some researchers used an IVTT system to synthesize EmrE and to reduce the problems of conventional technique [75, 76]. Although an IVTT system aid the synthesis of EmrE, preparation of functional EmrE remains an issue. Characterizing of EmrE and active transport of substrate usually require specialized and expensive devices [77, 78] with too high skilled handling [74, 77, 79]. Additionally, these are time consuming [76], costly and complicated procedure [80, 81-84].

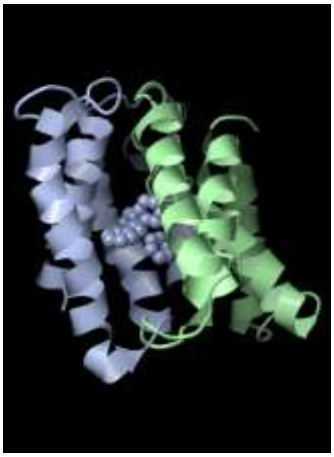

Fig. 16: Three-dimensional structure of EmrE. NMR structure of TPP bound EmrE is shown. Each monomer is shown in different color.

In this chapter, I synthesized, characterized, and quantified EmrE inside RB2 chamber. Firstly, I quantified the amount of AH at DIB by using the EtBr, one of the known

substrates of EmrE, diffusion through AH nanopore (as a positive control). Then, I quantified the amount of EmrE at DIB by using the EtBr. Finally, I tested the substrate specificity of EmrE by using specific and unspecific EmrE's substrate.

3-2 Material and Method

3-2-1 EmrE and E14C synthesis using a reconstituted IVTT system

EmrE and E14C (EmrE inactive mutant harboring mutation Glu to Cys at 14th residue) was synthesized by adding the corresponding PCR products to an IVTT system and incubated for 2 h at 37 °C. PCR product was prepared as described in 2-2-4. Finally, I confirmed the purity with an agarose gel electrophoresis (Fig. 17) and determine the concentration of the PCR product by nanodrop.

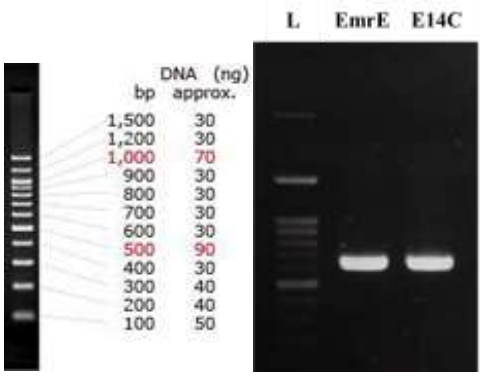

Fig.17: Gel electrophoresis for the PCR product of EmrE and E14C. I confirmed the purity of PCR product by performing agarose gel electrophoresis. The length of the products was as expected (630 bp). Nacalai DNA ladder broad range 100 bp was used as a DNA marker.

3-2-2 Functional assay of EmrE.

The fluorescence-based functional assay design is shown in Figs. 18 A and B. Firstly, RB2 chamber was filled with 14 µL of lipid dissolved oil [20 mg/mL DOPC in a mixture of 10:1 (v/v) hexadecane and decane], and two aqueous droplets of 3.5 µL were added to each position of RB2 chamber. The synthesis of EmrE occurred in the right droplet (IVTT system and 10 nM EmrE DNA (PCR product), while a substrate of EmrE, 2.5 µM ethidium bromide (EtBr), and a green fluorescence dye, bovine serum albumin conjugated to AlexaFluor 488 (BSA-A488) (66 kDa), were included in the left droplet. Given that EmrE requires a pH gradient for drug transport.[25] For that reason, the right droplet that contains IVTT system, the pH was adjusted to 7.6, whereas the left droplet, which contained most of the IVTT components except for the ribosome and tRNAs, the pH was adjusted to 8.1. After formation of the two contact droplet, the chamber was incubated on thermoplate at 37 °C for 2 h. Image recording every hour under fluorescence microscopy.

3-2-3 Data processing

Images were analysed using Image J to quantify the mean fluorescence intensity of each droplet as described in chapter 2, 2-2-6. To calculate the concentration of EtBr from the fluorescence of the droplet, EtBr with different concentration was added to the droplet containing a reconstituted IVTT system. This results in the emission of EtBr fluorescence upon the binding to nucleic acids present, *i.e.,* the ribosome and tRNAs. The correlation between EtBr and the fluorescence intensity of the droplet was plotted (Fig. 18). This standard curve was used to calculate the amount of EtBr which flowed into the adjacent droplet.

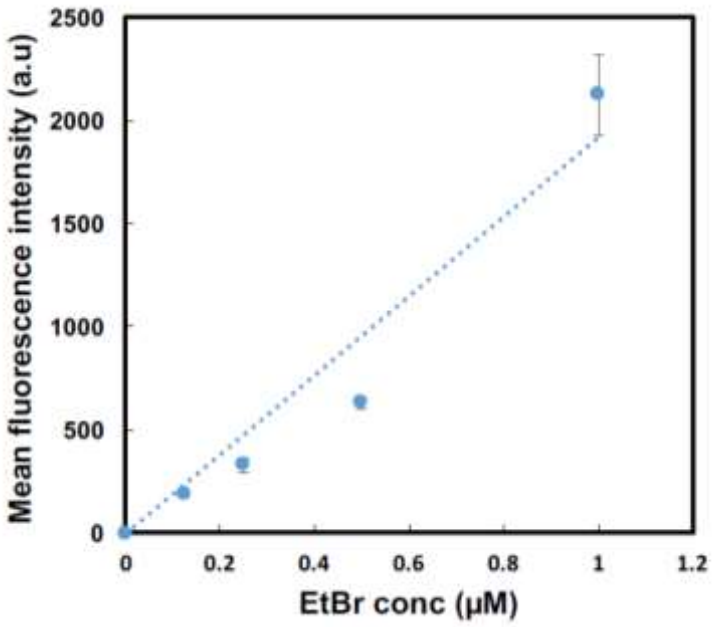

Fig. 18: Correlation between the EtBr concentration and fluorescence intensity inside the droplet. Different concentration of EtBr was added to the right droplet (Fig. 19A and B). The DIBs were prepared and observed under a microscope, and the fluorescence intensity was measured. The dashed line indicates the linear trendline.

3-3 Results

3-3-1 Quantifying the amount of AH at the DIB using EtBr

Firstly, AH was synthesized as a positive control, and the number of AH inserted at the DIB was quantified by using the intensity of EtBr fluorescence (Fig. 19B). As AH synthesized in the left droplet, a red fluorescence increased in the right droplet because of the EtBr diffusion. Red fluorescence emission in the right droplet due to the binding of EtBr to the nucleic acids present in an IVTT system, *i.e.* the ribosome and tRNAs (Fig. 19C). In contrast, the red fluorescence dye (BSA-A488) (66 kDa) in the right droplet could not pass through AH nanopore to the left droplet. From these results the presence

of AH nanopores has been confirmed. Notably, I observed the stability of droplets for at least 19 h. From the fluorescence data (Fig. 19D), The quantification method used for FDGlucU diffusion was applied to EtBr diffusion for calculating the amount of AH molecules inserted at the DIB. The correlation between the EtBr fluorescence and number of EtBr molecules was obtained (Fig. 18) and using $\boldsymbol{D}$ = 1.49 x 10^{-6} m^2 h^{-1} of EtBr [68], I calculated $\boldsymbol{J}$ = 1.245 mol m^{-2} h^{-1}. I then obtained $\boldsymbol{N_{pore}}$ = 0.176 x 10^5 heptamers per DIB at the bilayer. At last, the fraction of AH inserted into bilayer of the total amount of AH synthesized in the droplet (Fig. 23) was determined as 3.12 x 10^{-6} %. Interesting, the calculated value is very similar to that obtained with FDGlcU (2.44 x 10^{-6} %), indicating the validity of our measurement method.

3-3-2 Synthesizing EmrE inside the droplet

I tested the functional expression of EmrE from *E. coli* by a reconstituted IVTT system inside a stabilized DIB. I then investigated the uptake of EtBr by EmrE in the presence of a substrate of EmrE, *i.e.*, EtBr. Finally, I quantified the amount of EmrE at the DIBs.

Two 3.5 µL IVTT droplets were prepared and EmrE was synthesized in the right droplet, while 2.5 µM (EtBr), a substrate of EmrE, was added to the left droplet (Fig. 19A). Given that EmrE requires a pH gradient for drug transport [85], the pH of the right droplet was adjusted to 7.6, whereas the pH of the left droplet, which contained most of the IVTT components except for the ribosome and tRNAs, was adjusted to 8.1.

I then tested the EmrE synthesis by an IVTT system inside DIB and quantified the amount of EmrE inserted at the DIB (Fig. 19C). Only EmrE showed an increase in red

fluorescence while the inactive mutant of EmrE, E14C [85], didn't show. The emission of fluorescence in the right droplet due to binding of EtBr to the nucleic acids that present in the IVTT system. In the same time, BSA-A488 didn't penetrate the right droplet. These results suggest that the functional form of EmrE has been synthesized (Fig. 19C).

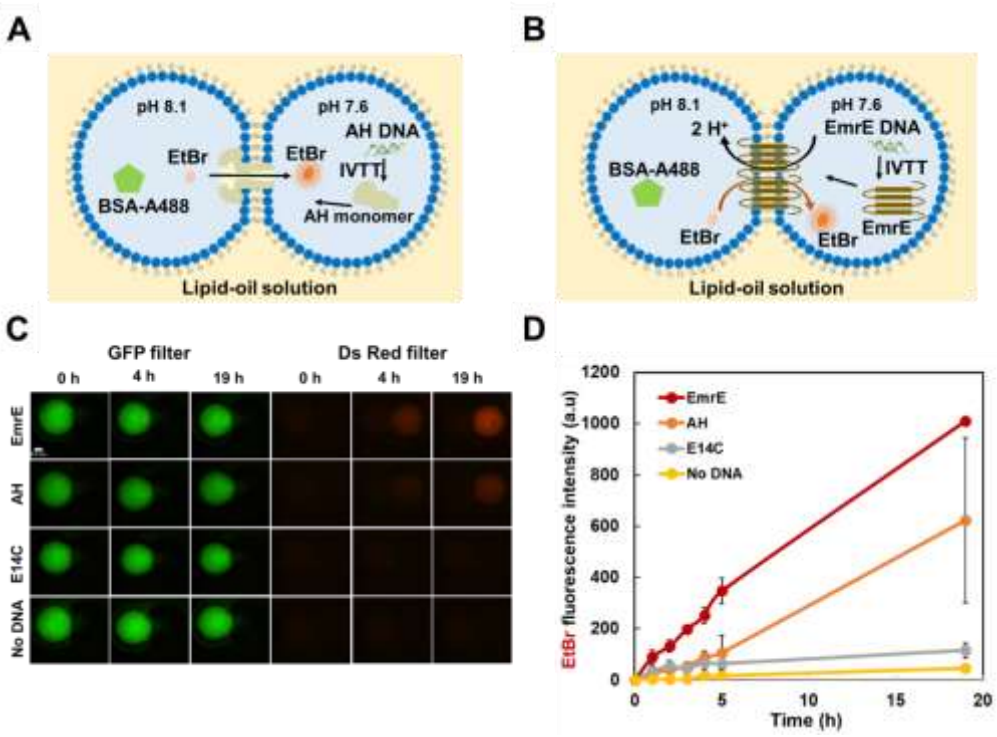

Fig. 19: EtBr diffusion and transport. (A) Schematic of EtBr transport by EmrE. (B) EtBr diffusion through AH pores across the DIB. (C) Representative images of the fluorescence-based functional assay of AH and EmrE. (D) Time course of EtBr fluorescence intensity (n = 3). Error bars indicate the standard deviation. The scale bar is 0.5 mm. The chamber was incubated at 37 °C for 2 h, and then at 25 °C. The time indicated is the total incubation time at 37 °C and 25 °C.

3-3-3 The pH gradient for EmrE and EtBr uptake

Previous studies reported that a pH gradient for EmrE is needed for the uptake of the substrate, *i.e.*, EmrE is a proton-drug antiporter. I investigated the effect of the pH gradient on the uptake of EtBr of EmrE. Two set of droplets have been prepared, one with pH gradient, where the left and right droplet has a pH of 8.1 and 7.6, respectively, while the other set with the same pH (pH 7.6) in both droplets. When EmrE was synthesized, I detected a stronger increase in red fluorescence in the presence of pH gradient (Fig. 20), indicating that observed transport of EtBr is caused by the proton-drug antiporter function of EmrE.

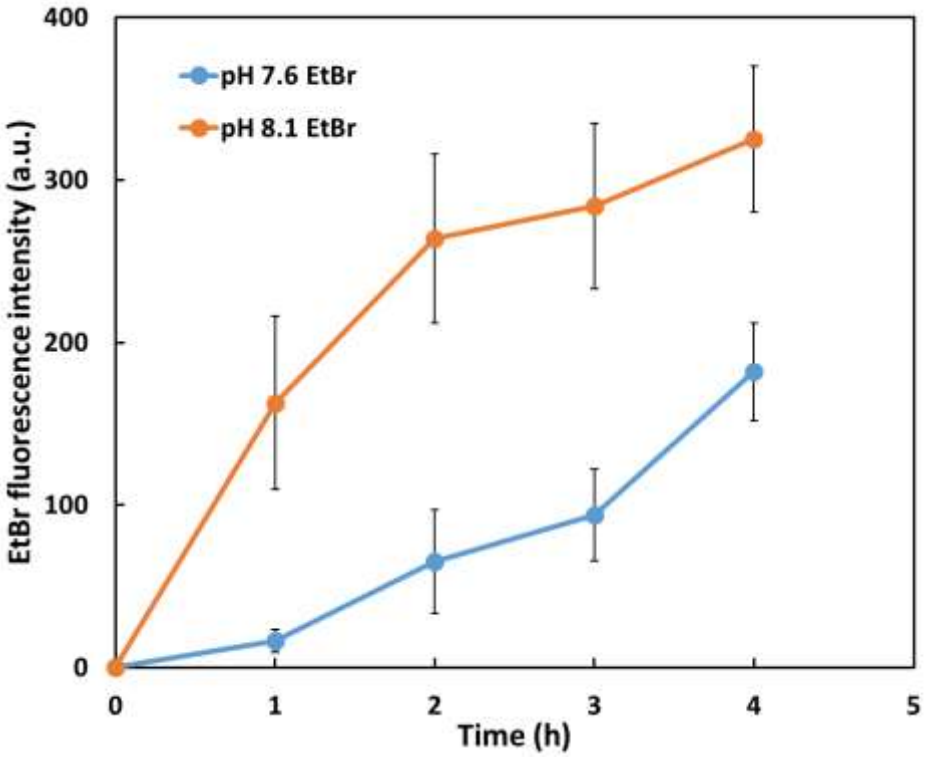

Fig. 20: The pH gradient affect EtBr influx by EmrE. Two set of droplets have been prepared, one with pH gradient, where the left and right droplet has a pH of 8.1 and 7.6, respectively, while the other set with the same pH (pH 7.6) in both droplets.

3-3-4 Specificity of substrate transport and the uptake of different substrates by EmrE

For further confirmation of the transport of EtBr is driven by the function of EmrE, I investigate the substrate specificity of EmrE. EmrE mostly transports cationic drugs from the cytoplasm, and thus chemicals like calcein (994 Da) should not be transported. When I investigated the transport of a mixture of calcein and EtBr, only the transport of EtBr was observed, and that of calcein was not observed even after 19 h incubation (Fig. 21).

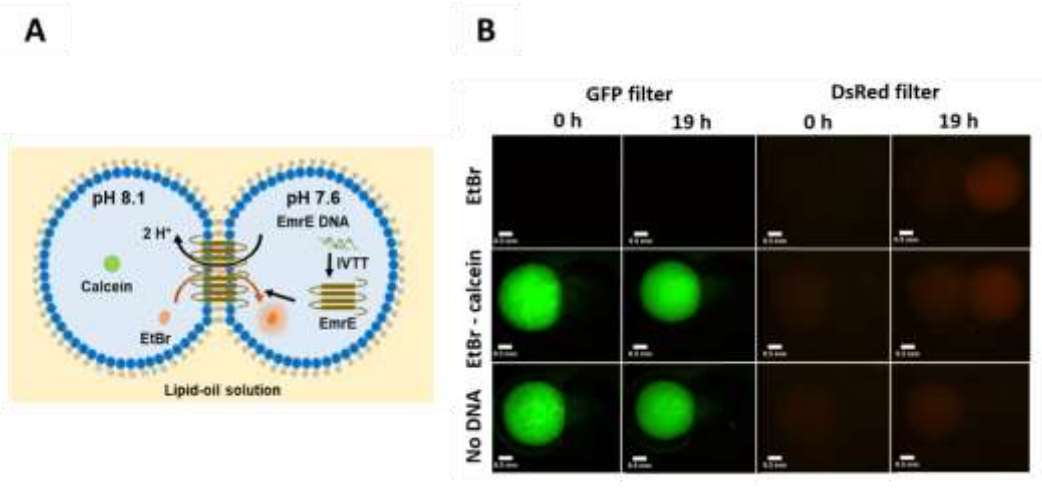

Fig. 21: Specificity of substrate transport by EmrE. (A) The left droplet contained 0.5 µM (EtBr), (a substrate of EmrE) and 10 µM calcein. EmrE was synthesized in the right droplet by a reconstituted IVTT. (B) Only the red fluorescence increased in right droplet while green fluorescence (calcein) remained in the left droplet.

Furthermore, competitive inhibition of EtBr transport was observed with another well-known substrate of EmrE, tetraphenylphosphonium (TPP^+). Different concentration of TPP^+ (0 µM, 5µM, 50 µM) was mixed with 2.5 µM EtBr, and the transport of EtBr was observed as depicted in (Fig. 22B). Both concentration of TPP^+ (5 µM and 50 µM)

showed inhibition of the red fluorescence, about 60% of EtBr intensity inhibited in the presence of TPP^+ (Fig.21C). I also confirmed that TPP^+ even at high concentration (50 µM) doesn't affect the GFP synthesis, and thus the decrease in the EtBr transport was not due to the inhibition of protein synthesis by TPP^+ (Fig. 23).

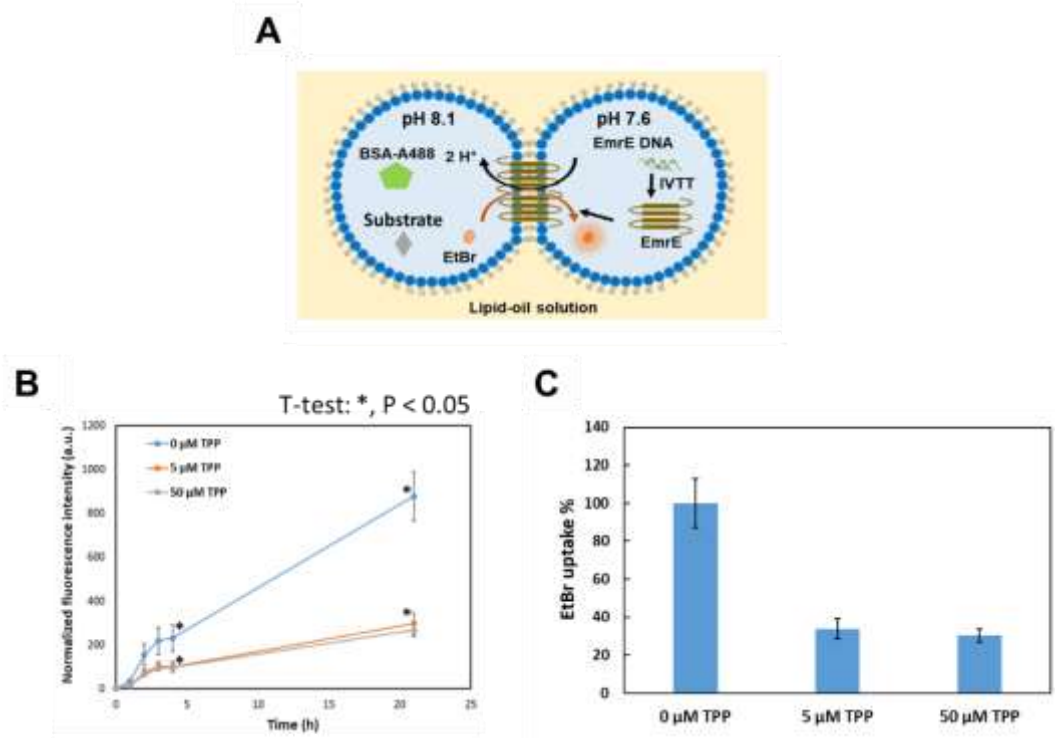

Fig. 22: Substrate compete with EtBr. (A) A mixture of EtBr and TPP was added to left droplet, and EmrE was synthesized in the right droplet by a reconstituted IVTT system. If competitive inhibition occurs, red fluorescence intensity will decrease in right droplet. (B) By adding TPP^+ with EtBr in left droplet, EtBr intensity decreased. (C) The uptake of different concentration of TPP^+ (5µM, 50 µM) showed inhibition of EtBr signal. Both concentration of TPP^+ (5 µM, 50 µM) have similar inhibition of EtBr signal.

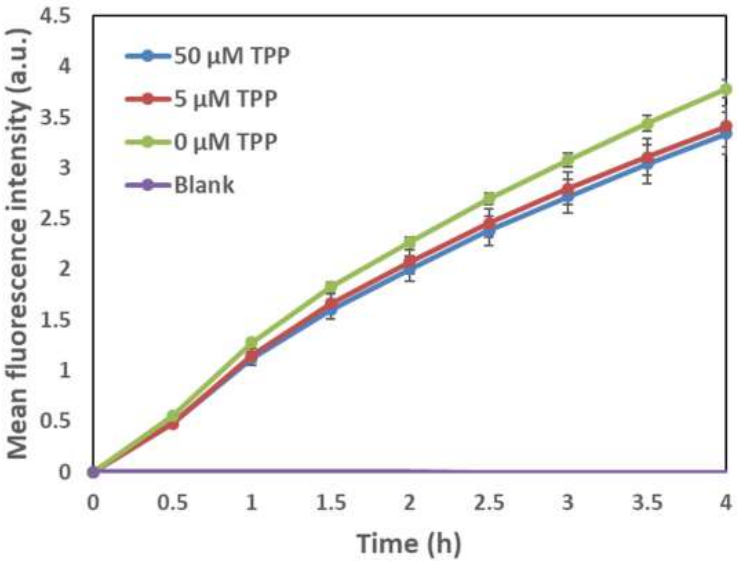

Fig. 23: GFP synthesis using a reconstituted IVTT system in the presence of TPP^+. Experiment was done essentially as described in Chapter 2, 2-2-1, except for the addition of TPP at indicated concentration. Average of 3 samples are plotted. Error bar indicates s.e.*m.*

3-3-5 Quantifying the amount of EmrE at the DIB

I quantified the amount of EmrE molecules inserted at the DIB. The rate of EtBr uptake by EmrE inside the DIB was determined as 1.19 x 10^9 EtBr molecules/min using the standard curve (Fig. 18). I assume that EmrE can transport EtBr at a rate of 7.5 nmol/min/µg, the same rate reported for methyl viologen [86], one of the popular substrates of EmrE, as corresponding value for EtBr has not been reported. From these values, the number of EmrE inserted into bilayer was determined as 52.4 × 10^5 dimers per DIB. I also determined the number of EmrE molecules synthesized in a droplet ($\boldsymbol{N}_{\mathrm{EmrE}}$ = 5.22 x 10^{12} dimer) (Fig. 24). Finally, the fraction of EmrE incorporated into DIB was found to be 1.0 x 10^{-4} % of the total amount of EmrE dimers synthesized inside droplet, which are 30- fold higher than that of AH. These results highlight that the values differ widely among the various MPs tested.

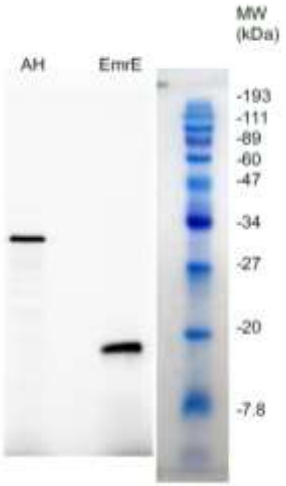

Fig. 24: Quantifying the amount of AH and EmrE synthesized using a reconstituted IVTT. AH and EmrE synthesis using IVTT was performed in the presence of [^{35}S]-methionine, with a DNA concentration of 10 nM at 37 °C for 2 h. The total amount of AH synthesized was quantified from SDS-PAGE, followed by autoradiography.

3-4 Discussion

This is the first report showing the expression of a multidrug transporter EmrE in functional form at the DIB and highlights the versatility of the system (Fig. 19). The rate of EtBr uptake inside the DIB by EmrE was obtained to be 1.2 x 10^9 EtBr molecules per min. While the inserted fraction of EmrE into DIB was found to be 1.0 x 10^{-4} % of the total amount of EmrE dimers synthesized. The fraction of AH incorporated into bilayer calculated with FDGlcU and EtBr were very similar. GFP protein synthesized by IVTT in PCR tube in the presence of TPP^+ with different concentration (0 µM, 5 µM, 50 µM), fluorescence signal decreased a little compared to 0 µM TPP^+(Fig. 23). I tested the uptake of different concentration of TPP^+ (5 µM, 50 µM) by EmrE. I observed the inhibition of EtBr signal in the present of each substrate (Fig. 22B).

A pH gradient is required for the active transport of substrate by EmrE. However, our result showed EtBr transported in the absence of pH gradient in slower manner. This transport could drive by transmembrane electrical potential which is one of the driving forces of the monovalent substrate (carried one positive charge) like EtBr. [66] Another factor affects the transport is the weak binding affinity of substrate at low pH difference. [82]

Chapter 4 General discussion and conclusion

This study aimed to establish a technique to study membrane protein inside DIBs. MPs have markable functions in biological system, that could be used as a tool to innovate biotechnological application such as biosensor and drug-screening. MPs should be maintained in its functional structure; however conventional techniques of MPs production and functional assay remain challenges. By using the described system in this study, I was able to synthesize MPs by a reconstituted IVTT system and quantified the number of MPs at the stabilized DIB. The developed chamber has been proved to aid in stabilizing the DIBs for at least 19 h. To show the potentiality of this method, I quantified two different type of MPs; the pore-forming protein α-hemolysin (AH) from *S. aureus* and the multidrug resistance EmrE from *E. coli*. Lastly, I confirm the inhibition of EtBr uptake by EmrE in the presence of competing substrates of EmrE. I aimed to use this method as a simple way for characterizing and quantifying various of MPs. Additionally, this method could develop to protein-based biosensor.

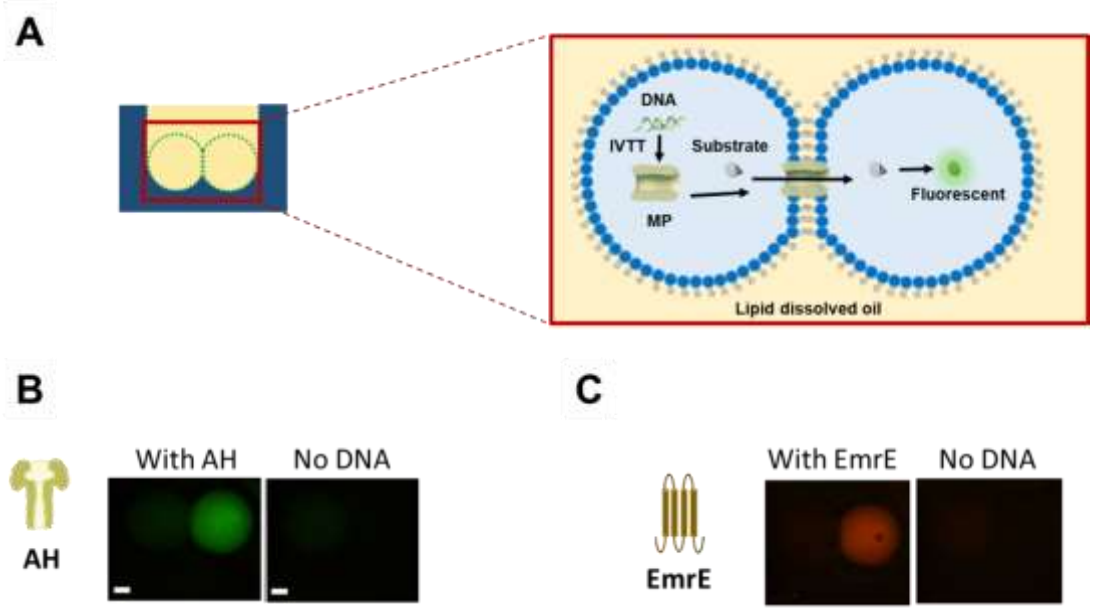

Fig. 25: General view of the functional assay achievement. (A) *In vitro* synthesis and characterization in DIBs made of IVTT system after stabilization by: Oil phase (mixture of hexadecane to decane) and chamber design (RB2 chamber). (B) *In vitro* synthesis, characterization, and quantification of the fraction of AH in stabilized DIB. (C) *In vitro* synthesis, characterization, and quantification of the fraction of EmrE inside DIB system.

In Chapter 2, I optimized the experimental condition to stabilize DIBs that consisted of a reconstituted IVTT system. The DIBs made of IVTT system affected by oil phase and chamber design. Whereas the oil mixture of 10:1 hexadecane to decane, enhance the DIB formation and minimized the oil in bilayer, resulting in relaxed interface and enhance the stability of the bilayer. While the chamber limited the movement and located the droplet and maintained the spherical shape by the round bottom design. Thereby synthesis of soluble MPs in the stabilized DIB has been followed. I succeeded in establishing the *in vitro* fluorescence-based functional assay with AH in the stabilized DIB inside RB2 chamber. I confirmed the formation of AH nanopore by the diffusion of FDGlcU to the other droplet where it was hydrolysed by GUS enzyme. The resulting green fluorescence

was measured and quantified to determine the percentage of AH inserted into bilayer to the total AH synthesized. I obtained N_{pore} = 4.8 x 10^4 heptamers per DIB. The percentage of AH inserted into bilayer was determined as 2.4 x 10^{-6} % of the total amount of AH synthesized inside the droplet. Low percentage might be due to the surface area to volume ratio and phospholipid composition affecting the insertion of MPs.

In Chapter 3, The synthesis of insoluble MPs in the stabilized DIB has been followed. I succeeded in establishing the in vitro fluorescence-based functional assay for insoluble MPs (EmrE). The amount of EmrE at the DIB quantified by similar way as described above. Additionally, I confirmed the specificity of EmrE substrate transport and that EmrE showed expected substrate specificity.

In the previous paper, the reported rate of methyl viologen, 7.5 nmol EtBr/min, is not clearly stated whether this value is a V_{max} (i.e., measured under substrate saturation condition) or not. The K_M value for methyl viologen has been reported as 260 μM, and thus is likely to reach a V_{max} around 500 μM. [87, 88] The EtBr concentration used in this study was 2.5 μM, 200-fold lower than 500 μM. This led to the possibility that the transport activity might be overestimated by 200-fold, leading to a significant underestimation of the amount of EmrE molecules at the DIB. Even after considering the underestimation of the amount of AH at the DIB and the EmrE at the DIB, our conclusions that (1) only a very small fraction (in the order of 10^{-2} to 10^{-6} %) is located at the DIB and (2) the amount of functional AH at the DIB is smaller than that of EmrE are not affected. In conclusion, this method showed the expression and characterization of soluble and insoluble MPs inside the IVTT DIB.

According to the calculation, the percentage of AH and EmrE incorporated into the bilayer was determined as 3.12 x 10^{-6} % and 1.0 x 10^{-4} % of the total amount of AH synthesized inside the droplet, respectively. That percentage was sufficient for detecting the function of MP. The density of MPs within the membrane of an *E. coli* cell is 1.7 x 10^5 molecules per μm^2, [87] while the density of AH at the DIB was 0.05 AH μm^{-2} and that for EmrE was 5.4 EmrE μm^{-2} , which are significantly lower than that of *E. coli*. The surface area to volume ratio of DIB (about 2.5 x 10^{-3} μm^{-1}) is smaller than that of *E. coli*. cell (about 4.7 - 7.8 μm^{-1}), consequence the collision between MPs and lipid bilayer inside the DIB is significantly lower than that inside *E. coli*. Thus, the molecules slowly reach the bilayer, suggested that only the MPs nearby the bilayer will insert. The phospholipid composition is another factor that could affect the number of MP at the DIB. That explains the 2-fold increase in the number of AH inserted at DIB by altering the lipid composition to 3 mix (DOPC, SM, CHO), since SM and PC are known to form clusters with cholesterol in supposed lipid rafts [51], that could affect the insertion of AH inserted into the bilayer. Lipid rafts work as condensation platforms for membrane-associated proteins; thus, it helps in the oligomerization of pore forming toxins [37, 51, 72, 89]. The lack of translocon machineries in DIBs is another factor could effect on the amount of MPs inserted at the DIBs. This percentage could be improved by investigating the experimental conditions, since AH function is known to be affected by other factors such as di-cation ions, or ADAM10 protein, resulting in dramatical decrease or increase in the fluorescence flux. It is possible to use the system to understand and characterize the function of MP by simply modifying the components and parameter.

Our developed system showed the potential of expressing and characterizing soluble (AH) and insoluble MP (EmrE) in its functional form, in addition to quantify the amount of inserted protein at DIB without using complicated techniques. The DIBs made of IVTT system were stabilized by optimizing the oil phase and chamber design. This method offers a new platform for characterizing MPs in a simple way and quantifying the protein depending on the fluorescence data. Moreover, the chambers are inexpensive, easy to use, cost effectively manufactured by injection molding (about $0.5 per chamber) and can be reused. Furthermore, unlike previous studies that made use of sophisticated apparatuses, such as nano injectors to prepare the DIB, [90, 91] the DIB in this device can be formed using a standard micropipette. Using the system presented here, provides us with a platform to further improve and understand how MPs are integrated efficiently into the lipid bilayer using a bottom-up approach. Furthermore, I showed the functional expression of EmrE at the DIB for the first time. The low value could be due to the low surface-to-volume ratio and the lack of translocon machineries. The introduction of membrane protein translocation machinery such as the Sec translocon [92, 93] and affinity-based concentration (i.e. nickel-modified lipid histidine tag and benzylguanine-modified lipid snap-tag [94]), may dramatically improve the sensitivity and/or detection time. Notably, EmrE can regulate the efflux of various toxic compounds [95-97], such as TPP^+, and thus, has the potential to act as a biosensor device [64, 69, 98-100] in the future.

References

[1] Reimhult, E., & Kumar, K. (**2008**). Membrane biosensor platforms using nano- and microporous supports. *Trends in biotechnology*, *26*(2), 82-89.

[2] Almeida, J. G., Preto, A. J., Koukos, P. I., Bonvin, A. M., & Moreira, I. S. (**2017**). Membrane proteins structures: A review on computational modeling tools. *Biochimica et Biophysica Acta (BBA)-Biomembranes*, *1859*(10), 2021-2039.

[3] Basheer, S., Samyn, D., Hedström, M., Thakur, M. S., Persson, B. L., & Mattiasson, B. (**2011**). A membrane protein-based biosensor: use of a phosphate–H+ symporter membrane protein (Pho84) in the sensing of phosphate ions. *Biosensors and Bioelectronics*, *27*(1), 58-63.

[4] Sachse, R., Dondapati, S. K., Fenz, S. F., Schmidt, T., & Kubick, S. (**2014**). Membrane protein synthesis in cell-free systems: from bio-mimetic systems to bio-membranes. *FEBS letters*, *588*(17), 2774-2781.

[5] Ayub, M., & Bayley, H. (**2016**). Engineered transmembrane pores. *Current opinion in chemical biology*, *34*, 117-126.

[6] Chalmeau, J., Monina, N., Shin, J., Vieu, C., & Noireaux, V. (**2011**). α-Hemolysin pore formation into a supported phospholipid bilayer using cell-free expression. *Biochimica et Biophysica Acta (BBA)-Biomembranes*, *1808*(1), 271-278.

[7] Schneider, B., Junge, F., Shirokov, V. A., Durst, F., Schwarz, D., Dötsch, V., & Bernhard, F. (**2010**). Membrane protein expression in cell-free systems. *Heterologous Expression of Membrane Proteins: Methods and*

Protocols, 165-186.

[8] Fujii, S., Matsuura, T., Sunami, T., Kazuta, Y., & Yomo, T. (**2013**). *In vitro* evolution of α-hemolysin using a liposome display. *Proceedings of the National Academy of Sciences*, *110*(42), 16796-16801.

[9] DiPilato, L. M., & Zhang, J. (**2010**). Fluorescent protein-based biosensors: resolving spatiotemporal dynamics of signaling. *Current opinion in chemical biology*, *14*(1), 37-42.

[10] Bayoumi, M., Bayley, H., Maglia, G., & Sapra, K. T. (**2017**). Multi-compartment encapsulation of communicating droplets and droplet networks in hydrogel as a model for artificial cells. *Scientific reports*, *7*, 45167.

[11] Bayley, H., Cronin, B., Heron, A., Holden, M. A., Hwang, W. L., Syeda, R., & Wallace, M. (**2008**). Droplet interface bilayers. *Molecular BioSystems*, *4*(12), 1191-1208.

[12] Holden, M. A., Needham, D., & Bayley, H. (**2007**). Functional bionetworks from nanoliter water droplets. *Journal of the American Chemical Society*, 129(27), 8650-8655.

[13] Funakoshi, K., Suzuki, H., & Takeuchi, S. (**2006**). Lipid bilayer formation by contacting monolayers in a microfluidic device for membrane protein analysis. *Analytical chemistry*, 78(24), 8169-8174.

[14] Nisisako, T., Portonovo, S. A., & Schmidt, J. J. (**2013**). Microfluidic passive permeability assay using nanoliter droplet interface lipid bilayers. *Analyst*, *138*(22), 6793-6800.

[15] Kawano, R., Tsuji, Y., Sato, K., Osaki, T., Kamiya, K., Hirano, M., ... &

Takeuchi, S. (2013). Automated parallel recordings of topologically identified single ion channels. *Scientific reports*, *3*, **1995**.

[16] Syeda, R., Holden, M. A., Hwang, W. L., & Bayley, H. (**2008**). Screening blockers against a potassium channel with a droplet interface bilayer array. *Journal of the American Chemical Society*, *130*(46), 15543-15548.

[17] Bayley, H.; Cronin, B.; Heron, A.; Holden, M. A.; Hwang, W. L.; Syeda, R.; Thompson, J.; Wallace, M. Droplet interface bilayers. Mol. BioSyst. **2008**, 4 (12), 1191−1208.

[18] Leptihn, S.; Castell, O. K.; Cronin, B.; Lee, E.-H.; Gross, L. C. M.; Marshall, D. P.; Thompson, J. R.; Holden, M.; Wallace, M. I. Constructing droplet interface bilayers from the contact of aqueous droplets in oil. Nat. Protoc. **2013**, 8 (6), 1048−1057.

[19] Punnamaraju, S.; Steckl, A. J. Voltage Control of Droplet Interface Bilayer Lipid Membrane Dimensions. Langmuir **2011**, 27 (2), 618−626.

[20] Schlicht, B., & Zagnoni, M. (**2015**). Droplet-interface-bilayer assays in microfluidic passive networks. *Scientific reports*, 5, 9951.

[21] Findlay, H. E., Harris, N. J., & Booth, P. J. (**2016**). In vitro synthesis of a Major Facilitator Transporter for specific active transport across Droplet Interface Bilayers. *Scientific reports*, *6*.

[22] Yanagisawa, M.; Yoshida, T.-a.; Furuta, M.; Nakata, S.; Tokita, M. Adhesive force between paired microdroplets coated with lipid monolayers. Soft Matter **2013**, 9 (25), 5891−5897.

[23] Baret, J.-C.; Kleinschmidt, F.; El Harrak, A.; Griffiths, A. D. Kinetic Aspects

of Emulsion Stabilization by Surfactants: A Microfluidic Analysis. Langmuir **2009**, 25 (11), 6088−6093.

[24] Zhang, F.; Proctor, A. Rheology and stability of phospholipidstabilized emulsions. J. Am. Oil Chem. Soc. **1997**, 74 (7), 869−874.

[25] Aguiar, H. B. d.; Beer, A. G. F. d.; Strader, M. L.; Roke, S. The Interfacial Tension of Nanoscopic Oil Droplets in Water Is Hardly Affected by SDS Surfactant. J. Am. Chem. Soc. **2010**, 132 (7), 2122− 2123.

[26] Venkatesan, G. A., Lee, J., Farimani, A. B., Heiranian, M., Collier, C. P., Aluru, N. R., & Sarles, S. A. (**2015**). Adsorption kinetics dictate monolayer self-assembly for both lipid-in and lipid-out approaches to droplet interface bilayer formation. *Langmuir*, *31*(47), 12883-12893.

[27] Challita, E. J., Najem, J. S., Monroe, R., Leo, D. J., & Freeman, E. C. (**2018**). Encapsulating networks of droplet interface bilayers in a thermoreversible organogel. *Scientific reports*, *8*(1), 1-11.

[28] Guiselin, B., Law, J. O., Chakrabarti, B., & Kusumaatmaja, H. (**2018**). Dynamic morphologies and stability of droplet interface bilayers. *Physical review letters*, *120*(23), 238001.

[29] Sumitomo, K., McAllister, A., Tamba, Y., Kashimura, Y., Tanaka, A., Shinozaki, Y., & Torimitsu, K. (**2012**). Ca^{2+} ion transport through channels formed by α-hemolysin analyzed using a microwell array on a Si substrate. *Biosensors and Bioelectronics*, 31(1), 445-450.

[30] Kleefen, A., Pedone, D., Grunwald, C., Wei, R., Firnkes, M., Abstreiter, G., & Tampé, R. (**2010**). Multiplexed parallel single transport recordings on nanopore arrays. *Nano letters*, 10(12), 5080-5087.

[31] Ota, S., Suzuki, H., & Takeuchi, S. (**2011**). Microfluidic lipid membrane formation on microchamber arrays. *Lab on a Chip*, 11(15), 2485-2487.

[32] Ganesan, P. V., & Boxer, S. G. (**2009**). A membrane interferometer. *Proceedings of the National Academy of Sciences*, 106(14), 5627-5632.

[33] Osaki, T., Watanabe, Y., Kawano, R., Sasaki, H., & Takeuchi, S. (**2011**). Electrical access to lipid bilayer membrane microchambers for transmembrane analysis. *Journal of microelectromechanical systems*, 20(4), 797-799.

[34] Castell, O. K., Berridge, J., & Wallace, M. I. (**2012**). Quantification of membrane protein inhibition by optical ion flux in a droplet interface bilayer array. *Angewandte Chemie International Edition*, 51(13), 3134-3138.

[35] Leptihn, S., Castell, O. K., Cronin, B., Lee, E. H., Gross, L. C., Marshall, D. P., & Wallace, M. I. (**2013**). Constructing droplet interface bilayers from the contact of aqueous droplets in oil. *Nature protocols*, 8(6), 1048-1057.

[36] Sarles, S. A., & Leo, D. J. (**2010**). Physical encapsulation of droplet interface bilayers for durable, portable biomolecular networks. *Lab on a Chip*, *10*(6), 710-717.

[37] Meesters, C., Brack, A., Hellmann, N., & Decker, H. (**2009**). Structural characterization of the α-hemolysin monomer from Staphylococcus aureus. *Proteins: Structure, Function, and Bioinformatics*, *75*(1), 118-126.

[38] Bhakdi, S., Füssle, R., & Tranum-Jensen, J. (**1981**). Staphylococcal alpha-toxin: oligomerization of hydrophilic monomers to form amphiphilic hexamers induced through contact with deoxycholate detergent micelles. *Proceedings of*

the National Academy of Sciences, *78*(9), 5475-5479.

[39] Stefureac, R., Long, Y. T., Kraatz, H. B., Howard, P., & Lee, J. S. (**2006**). Transport of α-helical peptides through α-hemolysin and aerolysin pores. *Biochemistry*, *45*(30), 9172-9179.

[40] Song, L., Hobaugh, M. R., Shustak, C., Cheley, S., Bayley, H., & Gouaux, J. E. (**1996**). Structure of staphylococcal α-hemolysin, a heptameric transmembrane pore. *Science*, 274(5294), 1859-1865.

[41] Vinothkumar, K. R., & Henderson, R. (**2010**). Structures of membrane proteins. *Quarterly reviews of biophysics*, *43*(1), 65-158.

[42] Bhakdi, S., & Tranum-Jensen, J. (**1991**). Alpha-toxin of Staphylococcus aureus. *Microbiology and Molecular Biology Reviews*, *55*(4), 733-751.

[43] Ropele, M., & Menestrina, G. (**1989**). Electrical properties and molecular architecture of the channel formed by Escherichia coli hemolysin in planar lipid membranes. *Biochimica et Biophysica Acta (BBA)-Biomembranes*, *985*(1), 9-18.

[44] Stanley, C. E., Elvira, K. S., Niu, X. Z., Gee, A. D., Ces, O., Edel, J. B., & Demello, A. J. (**2010**). A microfluidic approach for high-throughput droplet interface bilayer (DIB) formation. *Chemical communications*, *46*(10), 1620-1622.

[45] Tsuji, Y., Kawano, R., Osaki, T., Kamiya, K., Miki, N., & Takeuchi, S. (**2013**). Droplet split-and-contact method for high-throughput transmembrane electrical recording. *Analytical chemistry*, *85*(22), 10913-10919.

[46] Baxani, D. K., Morgan, A. J., Jamieson, W. D., Allender, C. J., Barrow, D. A.,

& Castell, O. K. (**2016**). Bilayer Networks within a Hydrogel Shell: A Robust Chassis for Artificial Cells and a Platform for Membrane Studies. *Angewandte Chemie International Edition*, *55*(46), 14240-14245.

[47] Bai, Y., He, X., Liu, D., Patil, S. N., Bratton, D., Huebner, A., ... & Huck, W. T. (**2010**). A double droplet trap system for studying mass transport across a droplet-droplet interface. *Lab on a Chip*, *10*(10), 1281-1285.

[48] Czekalska, M. A., Kaminski, T. S., Jakiela, S., Sapra, K. T., Bayley, H., & Garstecki, P. (**2015**). A droplet microfluidic system for sequential generation of lipid bilayers and transmembrane electrical recordings. *Lab on a Chip*, *15*(2), 541-548.

[49] Kawano, R., Osaki, T., Sasaki, H., Takinoue, M., Yoshizawa, S., & Takeuchi, S. (**2011**). Rapid detection of a cocaine-binding aptamer using biological nanopores on a chip. *Journal of the American Chemical Society*, 133(22), 8474-8477.

[50] Stefureac, R., Long, Y. T., Kraatz, H. B., Howard, P., & Lee, J. S. (**2006**). Transport of α-helical peptides through α-hemolysin and aerolysin pores. *Biochemistry*, *45*(30), 9172-9179.

[51] Shimizu, Y., Inoue, A., Tomari, Y., Suzuki, T., Yokogawa, T., Nishikawa, K., & Ueda, T. (**2001**). Cell-free translation reconstituted with purified components. *Nature biotechnology*, *19*(8), 751.

[52] Sunami, T., Sato, K., Matsuura, T., Tsukada, K., Urabe, I., & Yomo, T. (**2006**). Femtoliter compartment in liposomes for in vitro selection of proteins. *Analytical biochemistry*, 357(1), 128-136.

[53] Fujii, S., Matsuura, T., Sunami, T., Kazuta, Y., & Yomo, T. (**2013**). In vitro evolution of α-hemolysin using a liposome display. Proceedings of the National *Academy of Sciences*, 110(42), 16796-16801.

[54] Boreyko, J. B., Polizos, G., Datskos, P. G., Sarles, S. A., & Collier, C. P. (**2014**). Air-stable droplet interface bilayers on oil-infused surfaces. *Proceedings of the National Academy of Sciences*, *111*(21), 7588-7593.

[55] Taylor, G. J., Venkatesan, G. A., Collier, C. P., & Sarles, S. A. (**2015**). Direct *in situ* measurement of specific capacitance, monolayer tension, and bilayer tension in a droplet interface bilayer. *Soft matter*, 11(38), 7592-7605.

[56] Iwamoto, M., & Oiki, S. (**2015**). Contact bubble bilayers with flush drainage. *Scientific reports*, 5, 9110.

[57] Venkatesan, G. A., Lee, J., Farimani, A. B., Heiranian, M., Collier, C. P., Aluru, N. R., & Sarles, S. A. (**2015**). Adsorption kinetics dictate monolayer self-assembly for both lipid-in and lipid-out approaches to droplet interface bilayer formation. *Langmuir*, 31(47), 12883-12893.

[58] Gonzalez, M. R., Bischofberger, M., Pernot, L., Van Der Goot, F. G., & Freche, B. (**2008**). Bacterial pore-forming toxins: the (w)hole story? *Cellular and molecular life sciences*, *65*(3), 493-507.

[59] Culbertson, C. T., Jacobson, S. C., & Ramsey, J. M. (**2002**). Diffusion coefficient measurements in microfluidic devices. *Talanta*, *56*(2), 365-373.

[60] Yelin, R., Rotem, D., & Schuldiner, S. (**1999**). EmrE, a small Escherichia coli multidrug transporter, protects Saccharomyces cerevisiae from toxins by sequestration in the vacuole. *Journal of bacteriology*, *181*(3), 949-956.

[61] Hamada, T., & Yoshikawa, K. (**2012**). Cell-sized liposomes and droplets: real-world modeling of living cells. *Materials*, 5(11), 2292-2305.

[62] Niwa, T., Sasaki, Y., Uemura, E., Nakamura, S., Akiyama, M., Ando, M., & Akiyoshi, K. (**2015**). Comprehensive study of liposome-assisted synthesis of membrane proteins using a reconstituted cell-free translation system. *Scientific reports*, 5, 18025.

[63] Tsuji, Y., Kawano, R., Osaki, T., Kamiya, K., Miki, N., & Takeuchi, S. (**2013**). Droplet-based lipid bilayer system integrated with microfluidic channels for solution exchange. *Lab on a Chip*, 13(8), 1476-1481.

[64] Osaki, T., & Takeuchi, S. (**2017**). Artificial cell membrane systems for biosensing applications. *Analytical chemistry*, *89*(1), 216-231.

[65] Yerushalmi, H., Lebendiker, M., & Schuldiner, S. (**1995**). EmrE, an Escherichia coli 12-kDa multidrug transporter, exchanges toxic cations and H+ and is soluble in organic solvents. *Journal of Biological Chemistry*, *270*(12), 6856-6863.

[66] Rotem, D., & Schuldiner, S. (**2004**). EmrE, a multidrug transporter from Escherichia coli, transports monovalent and divalent substrates with the same stoichiometry. *Journal of Biological Chemistry*, *279*(47), 48787-48793.

[67] Ma, C., & Chang, G. (**2004**). Structure of the multidrug resistance efflux transporter EmrE from Escherichia coli. *Proceedings of the National Academy of Sciences*, *101*(9), 2852-2857.

[68] Morrison, E. A., & Henzler-Wildman, K. A. (**2014**). Transported substrate determines exchange rate in the multidrug resistance transporter EmrE. *Journal of Biological Chemistry*, *289*(10), 6825-6836.

[69] Misawa, N., Osaki, T., & Takeuchi, S. (**2018**). Membrane protein-based biosensors. *Journal of The Royal Society Interface*, *15*(141), 20170952.

[70] Mordoch, S. S., Granot, D., Lebendiker, M., & Schuldiner, S. (**1999**). Scanning cysteine accessibility of EmrE, an H+-coupled multidrug transporter from Escherichia coli, reveals a hydrophobic pathway for solutes. *Journal of Biological Chemistry*, *274*(27), 19480-19486.

[71] Dastvan, R., Fischer, A. W., Mishra, S., Meiler, J., & Mchaourab, H. S. (**2016**). Protonation-dependent conformational dynamics of the multidrug transporter EmrE. *Proceedings of the National Academy of Sciences*, *113*(5), 1220-1225.

[72] Gottschalk, K. E., Soskine, M., Schuldiner, S., & Kessler, H. (**2004**). A structural model of EmrE, a multi-drug transporter from Escherichia coli. *Biophysical journal*, *86*(6), 3335-3348.

[73] Cho, M. K., Gayen, A., Banigan, J. R., Leninger, M., & Traaseth, N. J. (**2014**). Intrinsic conformational plasticity of native EmrE provides a pathway for multidrug resistance. *Journal of the American Chemical Society*, *136*(22), 8072-8080.

[74] Morrison, E. A., DeKoster, G. T., Dutta, S., Vafabakhsh, R., Clarkson, M. W., Bahl, A., ... & Henzler-Wildman, K. A. (**2012**). Antiparallel EmrE exports drugs by exchanging between asymmetric structures. *Nature*, *481*(7379), 45-50.

[75] Elbaz, Y., Steiner-Mordoch, S., Danieli, T., & Schuldiner, S. (**2004**). In vitro synthesis of fully functional EmrE, a multidrug transporter, and study of its oligomeric state. *Proceedings of the National Academy of Sciences*, *101*(6), 1519-1524.

[76] Yerushalmi, H., Lebendiker, M., & Schuldiner, S. (**1996**). Negative dominance studies demonstrate the oligomeric structure of EmrE, a multidrug antiporter from Escherichia coli. *Journal of Biological Chemistry*, *271*(49), 31044-31048.

[77] Ong, Y. S., Lakatos, A., Becker-Baldus, J., Pos, K. M., & Glaubitz, C. (**2013**). Detecting substrates bound to the secondary multidrug efflux pump EmrE by DNP-enhanced solid-state NMR. *Journal of the American Chemical Society*, *135*(42), 15754-15762.

[78] Korkhov, V. M., & Tate, C. G. (**2008**). Electron crystallography reveals plasticity within the drug binding site of the small multidrug transporter EmrE. *Journal of molecular biology*, *377*(4), 1094-1103.

[79] Fitzgerald, G. A., Mulligan, C., & Mindell, J. A. (**2017**). A general method for determining secondary active transporter substrate stoichiometry. *Elife*, *6*, e21016.

[80] Gmeiner, W. H., Hudalla, C. J., Soto, A. M., & Marky, L. (**2000**). Binding of ethidium to DNA measured using a 2D diffusion-modulated gradient COSY NMR experiment. *FEBS letters*, *465*(2-3), 148-152.

[81] Steiner-Mordoch, S., Soskine, M., Solomon, D., Rotem, D., Gold, A., Yechieli, M., ... & Schuldiner, S. (**2008**). Parallel topology of genetically fused EmrE homodimers. *The EMBO journal*, *27*(1), 17-26.

[82] Adam, Y., Tayer, N., Rotem, D., Schreiber, G., & Schuldiner, S. (**2007**). The fast release of sticky protons: kinetics of substrate binding and proton release in a multidrug transporter. *Proceedings of the National Academy of Sciences*, *104*(46), 17989-17994.

[83] Robinson, A. E., Thomas, N. E., Morrison, E. A., Balthazor, B., & Henzler-Wildman, K. A. (**2017**). A kinetically-driven free exchange mechanism of EmrE antiport sacrifices coupling efficiency in favor of promiscuity. *bioRxiv*, 141937.

[84] Robinson, A. E., Thomas, N. E., Morrison, E. A., Balthazor, B. M., & Henzler-Wildman, K. A. (**2017**). New free-exchange model of EmrE transport. *Proceedings of the National Academy of Sciences*, *114*(47), E10083-E10091.

[85] Uyeda, A., Nakayama, S., Kato, Y., Watanabe, H., & Matsuura, T. (**2016**). Construction of an in vitro gene screening system of the E. coli EmrE transporter using liposome display. *Analytical chemistry*, *88*(24), 12028-12035.

[86] Elbaz, Y., Steiner-Mordoch, S., Danieli, T., & Schuldiner, S. (**2004**). In vitro synthesis of fully functional EmrE, a multidrug transporter, and study of its oligomeric state. *Proceedings of the National Academy of Sciences*, *101*(6), 1519-1524.

[87] Elbaz, Y., Tayer, N., Steinfels, E., Steiner-Mordoch, S., & Schuldiner, S. (**2005**). Substrate-induced tryptophan fluorescence changes in EmrE, the smallest ion-coupled multidrug transporter. *Biochemistry*, *44*(19), 7369-7377.

[88] Ninio, S., Rotem, D., & Schuldiner, S. (**2001**). Functional analysis of novel multidrug transporters from human pathogens. *Journal of Biological Chemistry*, *276*(51), 48250-48256.

[89] Kulma,M.; Herec,M.; Grudzinski,W.; Anderluh, G.; Gruszecki,W.I.; Kwiatkowska, K.; Sobota, A. Sphingomyelinrich domains are sites of lysenin oligomerization: Implications for raft studies. *Biochim. Biophys. Acta* **2010**, 1798, 471–481.

[90] Booth, M. J., Schild, V. R., Graham, A. D., Olof, S. N., & Bayley, H. (**2016**). Light-activated communication in synthetic tissues. *Science Advances*, *2*(4), e1600056.

[91] Leptihn, S., Castell, O. K., Cronin, B., Lee, E. H., Gross, L. C., Marshall, D. P., & Wallace, M. I. (**2013**). Constructing droplet interface bilayers from the contact of aqueous droplets in oil. *Nature protocols*, *8*(6), 1048-1057.

[92] Furusato, T., Horie, F., Matsubayashi, H. T., Amikura, K., Kuruma, Y., & Ueda, T. (**2018**). De novo synthesis of basal bacterial cell division proteins FtsZ, FtsA, and ZipA inside giant vesicles. *ACS synthetic biology*, *7*(4), 953-961.

[93] Ohta, N., Kato, Y., Watanabe, H., Mori, H., & Matsuura, T. (**2016**). In vitro membrane protein synthesis inside Sec translocon-reconstituted cell-sized liposomes. *Scientific reports*, *6*, 36466.

[94] Uyeda, A., Watanabe, T., Hohsaka, T., & Matsuura, T. (**2018**). Different protein localizations on the inner and outer leaflet of cell-sized liposomes using cell-free protein synthesis. *Synthetic Biology*, *3*(1), ysy007.

[95] Muth, T. R., & Schuldiner, S. (**2000**). A membrane-embedded glutamate is required for ligand binding to the multidrug transporter EmrE. *The EMBO journal*, *19*(2), 234-240.

[96] Ninio, S., Rotem, D., & Schuldiner, S. (**2001**). Functional analysis of novel multidrug transporters from human pathogens. *Journal of Biological Chemistry*, *276*(51), 48250-48256.

[97] Valeva, A., Hellmann, N., Walev, I., Strand, D., Plate, M., Boukhallouk, F., & Bhakdi, S. (**2006**). Evidence that clustered phosphocholine head groups serve

as sites for binding and assembly of an oligomeric protein pore. *Journal of Biological Chemistry*, *281*(36), 26014-26021.

[98] Ziesemer, S., Möller, N., Nitsch, A., Müller, C., Beule, A. G., & Hildebrandt, J. P. (**2019**). Sphingomyelin depletion from plasma membranes of human airway epithelial cells completely abrogates the deleterious actions of S. aureus alpha-toxin. *Toxins*, 11(2), 126.

[99] R. Syeda, M. A. Holden, W. L. Hwang and H. Bayley, J. Am. Screening blockers against a potassium channel with a droplet interface bilayer array. *Chem. Soc.*, **2008**, 130, 15543–15548.

[100] Castell, O. K., Berridge, J., & Wallace, M. I. (**2012**). Quantification of membrane protein inhibition by optical ion flux in a droplet interface bilayer array. *Angewandte Chemie International Edition*, *51*(13), 3134-3138.

List of Publication

- Elfaramawy, M. A., Fujii, S., Uyeda, A., Osaki, T., Takeuchi, S., Kato, Y., Watanabe, H. & Matsuura, T. (2018) Quantitative analysis of cell-free synthesized membrane proteins at the stabilized droplet interface bilayer, ***ChemCommun***. 54, 12226-12229.

Related publication

- Iwamoto, M., Elfaramawy, M. A., Yamatake, M., Matsuura, T. &Oiki, S. (2018) Concurrent *in Vitro* Synthesis and Functional Detection of Nascent Activity of the KcsA Channel under a Membrane Potential, ***ACS Synth Biol***. 7, 1004-1011.

Acknowledgements

First of all, I wish to express my sincere gratitude to **Professor Hajime WATANABE,** the school of Engineering at Osaka university, for providing me the opportunity to join Bioenvironmental Science (WATANABE Lab.).

I would like to express my great gratitude to my supervisor **Professor Tomoaki MATSUURA** for his generous support and the useful comments, remarks and engagement through the learning process of this master and PhD degree.

I also would like to thank **Assistant professor Yasuhiko KATO** for the support on the way. I sincerely thank **Research Assistant Atsuko UYEDA** for great assistance, and also thanks to all the members of Bioenvironmental Science (WATANABE Lab.) for their help during the period of my research.

I am greatly thankful to **Professor Shohi TAKEUCHI**, **Associate professor Toshihisa OSAKI**, and **Dr. Satoshi FUJII**, the University of Tokyo, for their comments that greatly improved the manuscript and for providing the chambers for the assay.

I am deeply grateful to **Professor Susumu UCHIYAMA** and **Professor Masahiro KINO-OKA**, Department of Biotechnology, Graduate School of Engineering, Osaka University, for their valuable comments and suggestions for writing and the thesis presentation.

Furthermore, I would like to acknowledge the Department of Biotechnology, Osaka University and Monbukagakusho (MEXT) Scholarship for financially supporting and for providing me the opportunity to enrol in this scholarship.

I also would like to thank **Professor Adel Hegazy**, (GEBRI), University of Sadat city, Egypt, for his support and encouragement.

Finally, I must express my very profound gratitude to my family; especially my husband Ali Faidallah, my mother, my spiritual inspiration; my father, and my brother Hisham Mahmoud for supporting and continuous encouragement through the process of researching and writing this thesis.